



Experiments to classify in-ground stilling basins and determine the factors affecting the optimization of flood mitigation dams

Ebi Meshkati^a, Sameh A. Kantoush^{b,*}, Tetsuya Sumi^b, Binh Quang Nguyen^{b,c,*} , Hossein Sohrabzadeh Anzani^b

^a Senior R&D Engineer Boskalis, the Netherlands

^b Water Resource Center, Disaster Prevention Research Institute (DPRI), Kyoto University, Kyoto 611-0011, Japan

^c The University of Danang - University of Science and Technology, 54 Nguyen Luong Bang, Danang, Vietnam

ARTICLE INFO

Keywords:

Flow energy
Cross-wall height
Hydraulic jump
Underground still basin
Sustainable flood management
Hydraulic infrastructure optimization

ABSTRACT

A "stilling basin" is a structure used downstream of a dam to reduce energy flow and prevent damage to the dam structure or erosion downstream. The literature on energy dissipation in stilling basins has identified mechanisms such as abrupt drops, sudden enlargements, steps, and cross walls. However, the combined effects of these mechanisms in a comprehensive experimental approach have not been thoroughly studied. This experimental study explores flow behavior within an in-ground stilling basin (ISB). In contrast to previous studies, this study systematically investigated the interaction between geometric parameters and flow behavior. Five types of hydraulic jumps were identified based on their surface patterns and water flow profiles. Among these, the steady submerged hydraulic jump is the most effective for reducing the flow velocity, maintaining stability, and ensuring symmetry. This study also highlights that the height of the cross-wall influences the flow pattern in the ISB more than variations in upstream conditions, such as the Froude number. Increasing the length of the ISB reduces the flow stability. Furthermore, incorporating free spaces in the ISB design improves flow stability and symmetry while offering additional benefits, such as better flushing efficiency, fish passage, and improved downstream flow conditions, which have not been fully addressed in prior studies. The results of this study provide the foundation for practical recommendations and design guidelines for ISBs in flood mitigation systems.

1. Introduction

The use of dams is a well-known strategy for controlling floods. The dams designed for controlling floods are called flood mitigation dams (FMDs), which are known as "dry dams" in the U.S. Kantoush et al. [1]. FMDs are the most eco-friendly flood control measures [2–4]. Under normal river conditions, an FMD allows the river to flow through its unobstructed bottom outlet. Conversely, when a flood occurs, a large percentage of the flood flow can be temporarily stored behind the dam [5]. Apart from the retarded flood flow behind the flood mitigation dam, the excess flow is discharged through the dam's bottom outlet to the downstream river during flood events. The outflow from the bottom outlet during a flood event is characterized by a high velocity depending on the water elevation behind the FMD. This high velocity could cause damage to downstream areas if the energy is not dissipated well. Therefore, it is necessary to dissipate the excess energy of the outflow to

reduce the risk of undesirable scouring, degradation, and failure of hydraulic structures. Various energy dissipation methods are available, including spillways [6–8], stilling basins, and hydraulic jumps. Each method has specific advantages depending on factors such as discharge rates, flow conditions, and the type of dam. Spillways typically handle large flows efficiently, whereas stilling basins combined with hydraulic jumps are commonly used to reduce the velocity and energy of high discharge rates in flood mitigation dams. A stilling basin combined with a hydraulic jump is thus vital for dissipating the energy of outflow from FMDs [3,4,9–11] (Fig. 1a–c).

A review of previous studies on hydraulic jumps revealed that the effects of design modifications, such as abrupt drops (e.g., [12,13–17]), sudden expansions (e.g., Kusnezow [18]; Hager [19–24]), cross walls on flow characteristics (e.g., [25]), and bed roughness (e.g., [16,21,26–32]), have been intensively investigated. These studies provide essential data that can be leveraged to develop machine-learning models

* Corresponding authors at: The University of Danang - University of Science and Technology, 54 Nguyen Luong Bang, Danang, Vietnam; Water Resource Center, Disaster Prevention Research Institute (DPRI), Kyoto University, Kyoto 611-0011, Japan.

E-mail addresses: kantoush.samehahmed.2n@kyoto-u.ac.jp (S.A. Kantoush), nqbinh@dut.udn.vn (B.Q. Nguyen).

<https://doi.org/10.1016/j.rineng.2025.104368>

Received 20 November 2024; Received in revised form 2 February 2025; Accepted 12 February 2025

Available online 13 February 2025

2590-1230/© 2025 The Author(s). Published by Elsevier B.V. This is an open access article under the CC BY license (<http://creativecommons.org/licenses/by/4.0/>).

for flood risk assessment and hazardous contaminant monitoring. By integrating these insights into predictive systems, more accurate flood management strategies can be designed, improving environmental safety and mitigation efforts during extreme flood events [33].

For an abrupt decrease, Ohtsu and Yasuda [14] argued that the supercritical-to-subcritical transition can have several flow patterns, depending on the inflow and tailwater flow conditions. They described four major flow patterns for abrupt drops via the s/h_1 ratio (s the drop height and h_1 supercritical depth on the drop) and the upstream Froude number, Fr_1 . They defined $0.5 \sim 1.5 \leq s/h_1 \leq 8 \sim 9$ as the low drop range and $s/h_1 \geq 15 \sim 16$ as the high drop range (Fig. 1c). Furthermore, the flow pattern changes from a low drop to a high drop when $s/h_1 \leq 0.5 \sim 1.5$, which is known as the free jump on the horizontal channel since the drop height (i.e., s/h_1) is small.

Concerning different inflow conditions, they proposed six types of jumps for flow behavior, including the A-jump, maximum wave jump, wave train jump, maximum B-jump, limited jump, and maximum plugging-type jump. Following Ohtsu and Yasuda [14], Mossa et al. [13] classified the types of hydraulic jumps by considering a broader range of influencing parameters. They constructed several charts based on the Froude number and subsequent flow depth and classified hydraulic jumps into the following types: A-jump, wave jump (W-jump), wave train jump, B-jump (or maximum plugging-type jump), and limited B-jump (also referred to as minimum B-jump). The limited B-jump refers to a weaker, less developed version of the B-jump that occurs under specific flow conditions, where the transition from supercritical to subcritical flow is less pronounced, and energy dissipation is reduced compared with a typical B-jump.

Kusnezow [18] conducted the first experiments on suddenly expanding channels by experimenting with S-jumps ($Fr_1 = 7.25$). The hydraulic jump characteristics in a nonprismatic rectangular channel were evaluated by Hager [19]. He sought to determine logical hydraulic approaches for gradual and abrupt channel enlargement jumps. For identical inflow conditions, the efficiency of the hydraulic jump was greater for a symmetric abruptly enlarged channel than for a rectangular prismatic channel. He suggested that the longitudinal component of hydraulic jumps in horizontal channels is quite unstable and that some irregularities at the bottom, such as sills, positive or negative steps, or other chicanes, can contribute to better stabilization. The classification of the flow behavior downstream of a sudden expansion in a rectangular channel was performed by Bremen and Hager [20] for different inflow conditions. The categories are repelled jump (R-jump), spatial jump (S-jump), transitional jump (T-jump), and classical hydraulic jump. Based on their results, S-jumps are unacceptable in terms of efficiency and length. Hence, they were concentrated on the T-jumps where the toe is upstream of the expansion section. They illustrated the greater efficiency of T-jumps compared with the corresponding classical hydraulic jump.

Additionally, T-jumps require less tailwater depth. They concluded that efficient T-jumps do not satisfy the compactness and symmetry requirements. Therefore, it is necessary to use additional baffles and terminals for comprehensive energy dissipation in T-jumps. Ohtsu et al. [15] reported submerged jumps below a sudden expansion. They categorized submerged jumps into asymmetric submerged jumps (ASJs), periodically submerged jumps (PSJs), and steady submerged jumps (SSJs). They reported that SSJs might be the most desirable flow pattern

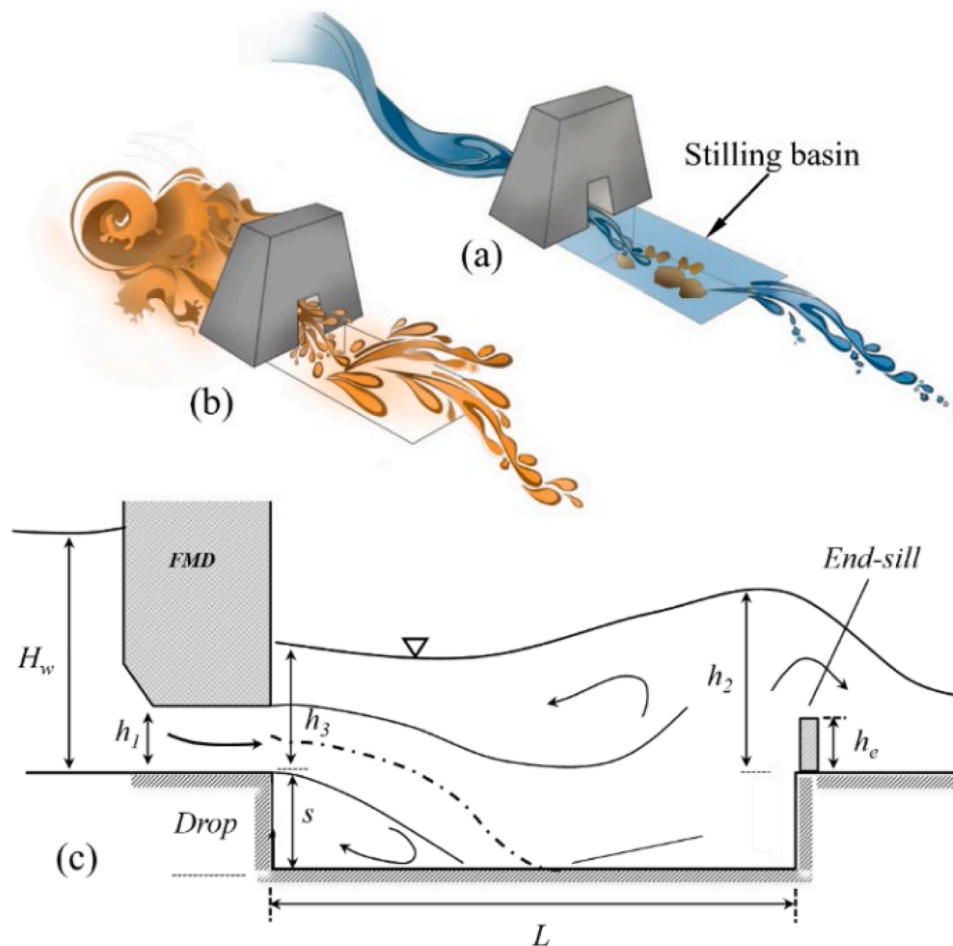


Fig. 1. Schematic representation of a flood mitigation dam illustrating three stages: (a) the dam's configuration before the flood event, (b) its behavior during the flood event, and (c) a side view of the underground stilling basin, including relevant geometric and hydraulic parameters.

owing to their stability and symmetrical behavior. According to their results, the flow pattern of a stilling basin relies on geometric parameters (e.g., the expansion ratio) rather than the inflow Froude number. They tested a wide range of experimental conditions but ignored the effect of the number of drops at the cross-wall height on the energy dissipation of a stilling basin.

When the tailwater depth is less than the CHJ, the basin length increases, and the toe of the jump moves downstream of the inlet gate. Accessories, such as drops, expansions, sills, baffles, blocks, and steps, are used in the basin to control jumps, reduce basin length, and stabilize the jump toe position (Chanon [34]). CHJs affected by accessories are called forced hydraulic jumps (FHJs), as Zare and Doering [24] suggested. FHJs have been widely studied by Bradley and Petreka [35], Rajaratna and Hurting [36], Debabeche et al. [37], Zare et al. [24], and Maatooq and Taleb [38]. In a laboratory study, Zare and Doering [24] tested forced submerged hydraulic jumps in prismatic and nonprismatic stilling basins. They adopted two expansion ratios, and a critical design case was established using different solid sill heights and locations. As the Fr number increased, the effect of sills on the energy dissipation efficiency decreased. The effect of sills on energy dissipation was greater for symmetric expansion than for asymmetric expansion. The asymmetric expansion basin was longer than the symmetric basin. They concluded that the length could be slightly reduced compared with that of Ohtsu et al. [15] using sills in the stilling basin.

Many studies have focused on the effect of bed roughness on hydraulic jumps, the earliest of which might be Rajaratnam [32]. The authors suggested that the tailwater depth (y_2) is much shallower than the subsequent depth estimated by the Belanger equation for rough beds. Furthermore, he argued that the jump length on rough beds was significantly shorter than on classical beds. A theoretical and experimental study was conducted by Ead and Rajaratnam [29] on hydraulic jumps on a corrugate bed at a predefined range of Froude numbers ($4 \leq Fr_1 \leq 10$). The jump length on the corrugated bed was half that on the smooth bed. They also revealed that the tailwater depth required for a hydraulic jump over a corrugated bed is smaller than that required for a smooth bed, and the jump length was half that of a smooth bed. Carollo et al. [28] used gravels and cobbles of different diameters to assess the hydraulic jump over homogenous and nonhomogeneous rough beds. The results indicated that boundary roughness reduced a hydraulic jump's sequential depth and length.

Parsemeh et al. [16] investigated the specifications of hydraulic jumps over rough beds with an uncontentious roughness element of lozenge shape over adverse slopes. Their experimental efforts revealed that rough elements could stabilize jumps over adverse slopes because they act as depressions in the bed and increase the bed shear stress by forming eddies. The relative energy loss exceeded the classic hydraulic jump over a horizontal bed. Mahtabi et al. [39] conducted experimental research to evaluate the effects of different expansion ratios on pressure fluctuations during a spatial hydraulic jump on a rough bed. Based on the Froude number, they categorized hydraulic jumps over naturally and artificially rough beds via a decision tree and neural network classifiers. Türker and Valyrakis [40] evaluated and measured the influence of channel bed roughness on hydraulic jumps. As the bed roughness increased, their results revealed that the shear force coefficient could remain the same, provided that the modified Reynolds number increased. In that case, the number of eddies increases in the flow, and consequently, the resisting forces are amplified. They reported that increased representative sand and gravel sizes induced a reduction in the conjugate depth ratio during the hydraulic jump. Bai et al. [41] experimentally studied hydraulic jumps with identical inflow Froude numbers over smooth beds, fully or partially grated rough beds, and partially vegetated grate-rough beds covered with artificial plants of different densities. They noted that bottom vegetation caused upward deflection of the hydraulic jump roller, reducing the jump length and increasing the jump free-surface slope. They reported that the effects of flexible vegetation on the conjugate depth ratio seemed insignificant compared

with those of rigid bottom roughness. Hasani et al. [21] investigated the effect of bed roughness on the pressure fluctuations of S-jumps with different expansion ratios and reported that the pressure fluctuations of S-jumps with different expansion ratios decreased as the roughness increased. They also reported that the energy loss increased, and the pressure fluctuation intensity decreased because lateral vortices formed in a sudden expanding section.

Studies have extensively investigated abrupt decreases, sudden increases, positive steps, and crosswalks in the literature. However, the combined effects of an abrupt drop, sudden enlargement, an end-positive step, and a cross-wall on the flow pattern and flow dissipation processes within a stilling basin have not been thoroughly examined. The characteristics of forced submerged hydraulic jumps in such a complex geometry remain largely unexplored. To address this gap, the present study experimentally investigates the behavior of a newly proposed type of stilling basin (SB), referred to as the ISB (Fig. 1c). More specifically, this study aims (i) to classify the different flow patterns that can occur within an ISB, (ii) to identify the key non-dimensional, and (iii) to propose design parameters for evaluating the optimal flow pattern. The ISB is a nonprismatic SB that integrates a sudden transverse enlargement with an abrupt vertical drop at its upstream end, where the bottom outlet of the flood mitigation dam (FMD) is located. The research methodology involved detailed experimental testing to observe and measure the flow behavior within the ISB under various conditions. The study analyzed how changes in geometry (e.g., sudden enlargement and drop height) influence flow patterns, energy dissipation, and the overall performance of the ISB. The findings provide a basis for practical recommendations and design guidelines to optimize ISBs downstream of flood mitigation dams, offering valuable insights into their hydraulic efficiency and energy dissipation capabilities.

2. Experimental investigation

2.1. Model setup

The experiments were conducted at Ujigawa Open Hydraulic Laboratory, Disaster Prevention Research Institute (DPRI), Kyoto University, Japan. A rectangular horizontal flume with a length of 11 m, width of 0.5 m, and height of 0.5 m was used (Fig. 2a–e). The flume bottom was made of metal sheets, and the walls were made of laminated glass to observe the flow behavior. The dimensions of this physical model were designed based on the average dimensions of the actual stilling basin of three FMDs (dray dams) in Japan, namely, Masudagawa, Tsuzuki, and Mogamioguni (Fig. 2f).

This implies a scale factor for a length of 1/40. Froude similarity was used to reduce the scale of the hydraulic parameters. For these FMDs, a 100-year flood return period results in Froude numbers ranging from 3 to 6 at the bottom outlet. Thus, Froude numbers in this range may ensure that gravity forces are scaled in the physical model. The scale ratio of the lengths from the prototype to the physical model was chosen by assuming the width of the ISBs in the laboratory. The physical model setup consists of a rectangular ISB with inner dimensions of 0.5 m width and variant lengths of 0.65–1.4 m (Table 1). After the cross wall of the ISB, the water level is controlled by a flap gate at the end of the channel outlet. A 2-meter-long, movable frame is mounted along the channel sidewalls to carry the instrument devices.

2.2. Investigated ISB geometries and measuring devices

A total of 30 experiments were conducted corresponding to 10 symmetric ISBs with different depths, lengths, cross-wall heights, and widths. Experiments were conducted for different Froude numbers, and the effects of the ISB step drop and length and the cross-wall height on the flow characteristics were studied. The tested ISB geometries and hydraulic conditions are listed in Table 1.

Table 1 summarizes the tested ISB configurations under different ISB

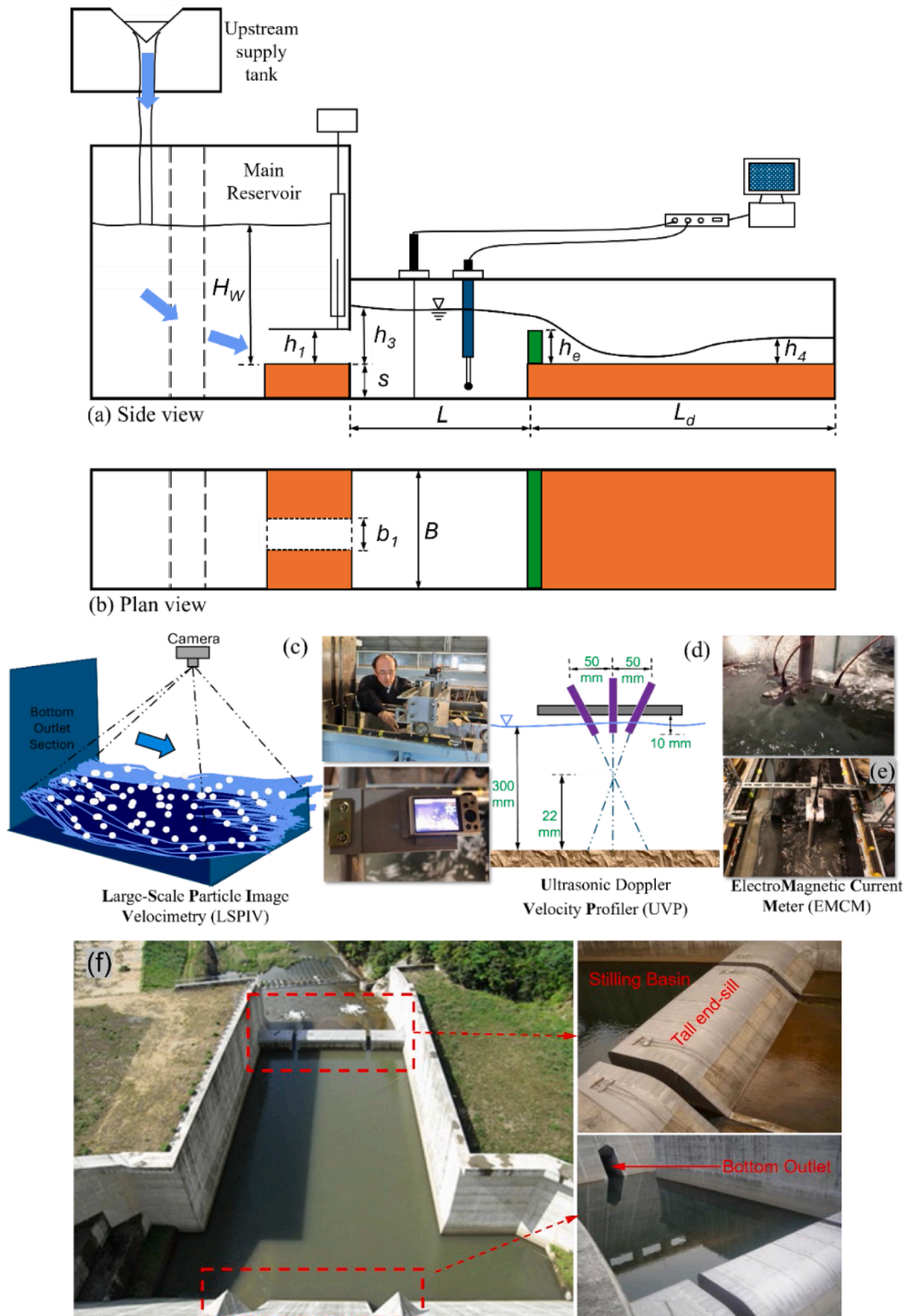


Fig. 2. Illustration of the experimental setup: (a) side view and (b) plan view. (c) – (e) The measuring devices used are a large-scale particle image velocimeter (LSPIV), an ultrasonic Doppler velocity profiler (UVP), and an electromagnetic current meter (EMCM). (f) The stilling basin of Masudagawa Reservoir, Japan.

lengths of 75, 100, and 125 cm and various step depths of 5, 10, and 15 cm. For each ISB geometry configuration, different end sill geometries with heights of 0, 4, 8, 12, and 13.5 cm were systematically examined to determine the optimum case. The end-sills were placed vertically above the positive step and perpendicular to the longitudinal axis of the flume. End sill widths of 50, 40, 30, and 20 cm were also investigated to explore

the effect of free space on both sides of the end sill. In addition to the three different Froude numbers of supercritical flow at the bottom outlet (namely, $Fr_1 = 2.8, 4.9, \text{ and } 5.1$), only one dimension of the bottom outlet ($h_1 = 5 \text{ cm}$ and $b_1 = 10 \text{ cm}$) was examined, thus creating an expansion ratio of $k = 0.2$ ($k = b_1/B$), similar to the average practical expansion ratio for FMDs.

Table 1
Designed dimensions of the physical model used in the present research.

Item	Prototype	Physical model	Scale factor
ISB length [m]	26–56	0.65–1.40	40
ISB width [m]	20	0.50	40
Drop height [m]	1–4	0.025–0.100	40
Bottom outlet height [m]	1.9–3.4	0.0475–0.085	40
Bottom outlet width[m]	1.7–4.45	0.0425–0.111	40
Discharge [m^3s^{-1}]	40–320	0.0039–0.031	40

The geometry of the physical model of ISBs (e.g., depth and length) could be changed systematically using prepared wooden pieces glued to the physical model body. A centrifugal pump and pipe were employed to support the recirculation of water. During the experiments, discharge was controlled by a calibrated 90-degree V-notch weir upstream of the model setup (Fig. 2a).

To monitor the fluctuations in water depth along the ISB, an electromagnetic water level meter (produced by JFE ADVANTEC, Japan) was used (Fig. 2e). The water level at three cross-sections was measured, namely, at the face of the dam outlet (cross-section I), at the cross-wall (cross-section II) and downstream of the cross-wall (cross-section IV). At each cross-section, four different points were measured, and the average value of the water level was used for data analysis. The sampling frequency and the number of samples taken for each point were set to 50 Hz

and approximately 32,000, respectively. The hydraulic jump characteristics were recorded through observation, photography, and recording of high-resolution movies from the top and side, owing to the Plexiglas sidewall of the flume. In addition, 2D surface velocity and 3D velocity profiles are measured via large-scale particle image velocimetry (LSPIV) and ultrasonic Doppler velocity profiler (UVP) devices, respectively (Fig. 2c and d).

2.3. Experimental conditions and dimensional analysis

The simplest and most popular hydraulic jump is on a smooth horizontal floor within a rectangular channel, which various scholars have extensively studied. Following De Padova and Mossa [42], Bidon conducted one of the first experimental analyses of hydraulic jumps in 1820. Based on his experiments conducted with varying discharge rates, an equation describing the behavior of hydraulic jumps was proposed, as shown in Eq. 1.

$$y_2 - y_1 = \frac{V_1^2 - V_2^2}{2g} \tag{1}$$

where y_1 and y_2 are the upstream and downstream depths (or elevation heads), respectively, representing the initial and subsequent flow depths. V_1 and V_2 are the supercritical (or upstream) and downstream

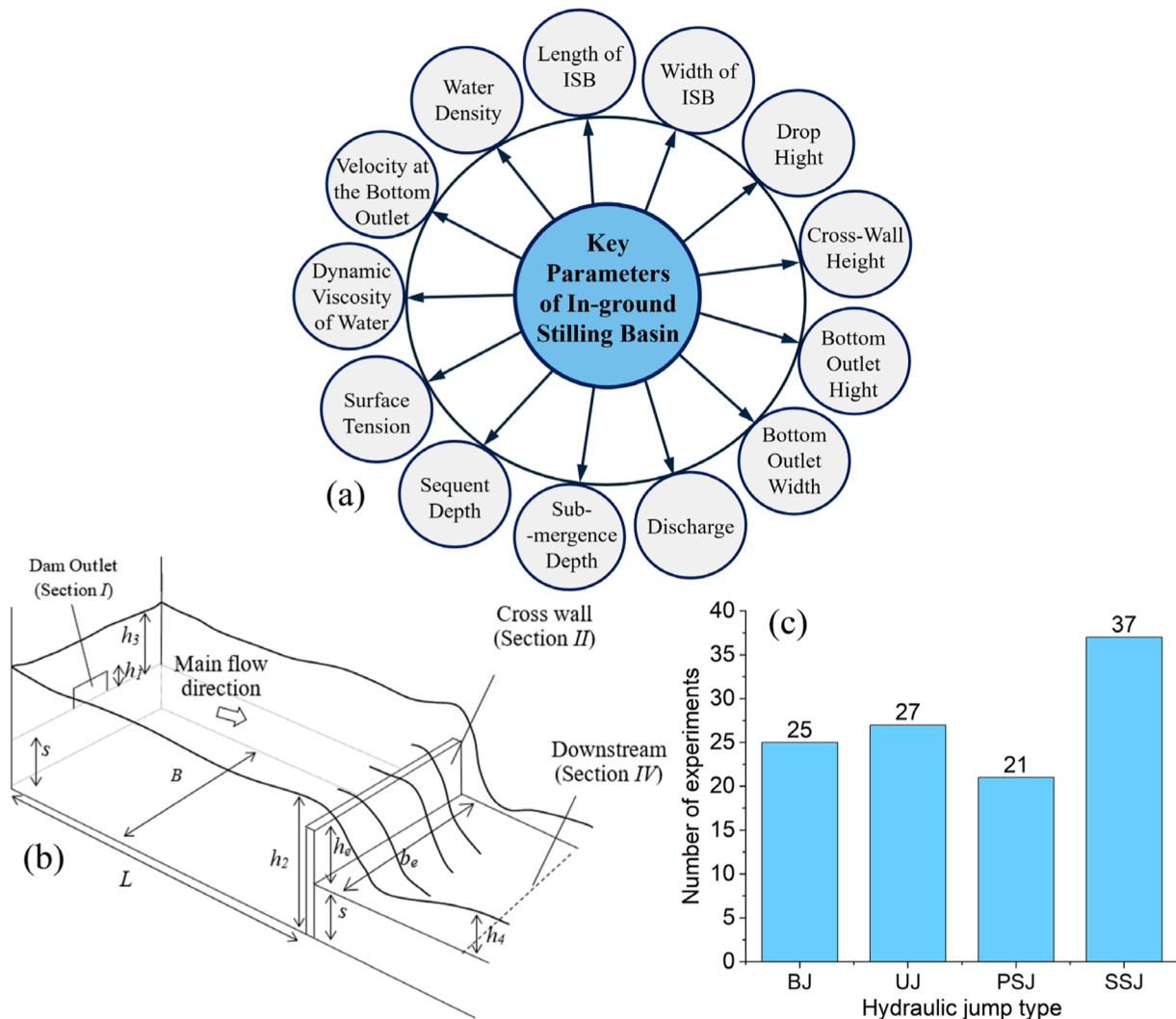


Fig. 3. (a) Key parameters governing the hydraulic performance of the ISBs. (b) Schematic diagram of the experimental model used in this study. (c) Number of experiments for each hydraulic type.

velocities, respectively.

De Padova and Mossa [42] mentioned that early researchers, including Bélanger and Bidon, developed equations based on continuity and momentum for a rectangular channel with a smooth horizontal bed. Based on their findings, an equation was proposed to estimate the subsequent depth ratio, as presented in Eq. 2.

$$\frac{y_2}{y_1} = \frac{1}{2} \left(\sqrt{1 + 8Fr_1} - 1 \right) \quad (2)$$

where $Fr_1 = V_1/\sqrt{gy_1}$ is the Froude number.

Fig. 3a and b illustrate a key parameter and a schematic view of an ISB. The hydraulic performance (HP) of the ISB is governed by the following parameters, as shown in Eq. 3:

$$HP = f(U_o, b_1, h_1, h_2, h_3, s, b_e, B, L, h_e, Q, g, \sigma, \rho, \mu) \quad (3)$$

where U_o is the outlet velocity at the bottom outlet face, b_1 is the bottom outlet width, h_1 is the bottom outlet height, h_2 is the sequent depth (the downstream flow depth following the hydraulic jump in the ISB), h_3 is the submergence depth, s is the drop height, b_e is the effective width of the end sill, B is the ISB width, L is the ISB length, h_e is the cross wall height, Q is the discharge, ρ is the water density, σ is the surface tension, μ is the dynamic viscosity of water, and g is the gravitational acceleration.

Using dimensional analysis, the parameters of Eq. (3) are reduced to Eq. (4):

$$HP = f\left(Y_2, Y_3, \frac{s}{h_1}, \frac{L}{B}, k, a, \frac{h_1}{B}, \frac{h_e}{h_c}, \frac{b_e}{B}, W, Re, Fr_1\right) \quad (4)$$

Here, Y_2 is the ratio of the sequential depth to the bottom outlet height (h_2/h_1), Y_3 is the degree of submergence or, in other words, the ratio of the water depth at the face of the bottom outlet to the bottom outlet height (h_3/h_1), k is the expansion ratio (b_1/B), a is the outlet aspect ratio (h_1/b_1), h_c is the critical depth, defined as the depth of flow

at which the specific energy is minimized for a given discharge $\left(\frac{Q^2}{B^3g}\right)^{\frac{1}{3}}$,

L/B is the ISB aspect ratio, s/h_1 is the drop number, and h_e/h_c is the normalized cross-wall height. Moreover, the Weber number (W) is defined as $W = \frac{\rho LU_o^2}{\sigma}$ (Abdi Chooplou et al. [43], [44–46]). The Reynolds number (Re) is expressed as $Re = \frac{\rho U_o h_1}{\mu}$ [47,48,49].

The dimensions of the bottom outlet ($h_1 = 5$ cm and $b_1 = 10$ cm) and the width of the ISB ($B = 50$ cm) were constant. This implies a constant expansion ratio ($k = b_1/B$) of 0.2 and a given outlet aspect ratio ($a = h_1/b_1$) of 0.5, which engineers commonly use at commercial field scales.

Kiani et al. [50] reported that the effect of viscosity is insignificant when $Re > 10,000$. Heller [51] also suggests a minimum value of 110 for its square root of W . In this study, $\sqrt{W} > 110$ and elimination from Eq. (4) is used. Therefore, the normalized hydraulic performance (NHP) of the ISB can be expressed as follows in Eq. 5:

$$NHP = f\left(Y_2, Y_3, \frac{s}{h_1}, \frac{b_e}{B}, \frac{L}{B}, \frac{h_e}{h_c}, Fr_1\right) \quad (5)$$

Fig. 3c and Table 2 present the number of tests for each type of hydraulic jump. The nondimensional parameters of the 110 experiments that were conducted are presented in Table 2.

Table 2
Nondimensional test parameters.

Fr_1	L/B	s/h_1	h_e/h_c	Y_2	Y_3	Jump types	No. Exp.
2.85–4.99	1.5, 2, 2.5	1, 2, 3	0–0.75	2.17–5.28	0.25–1.18	BJ	25
2.85–4.99	1.5, 2, 2.5	1, 2, 3	0.75–2.66	2.99–6.10	1.05–3.22	UJ	27
2.85–4.99	1.5, 2, 2.5	1, 2, 3	1.50–3.52	3.83–6.94	2.21–3.64	PSJ	21
2.85–4.99	1.5, 2, 2.5	1, 2, 3	1.50–3.97	4.71–7.09	2.41–3.92	SSJ	37
Total No. Experiment							110

In this table, the BJ, UJ, PSJ, and SSJ correspond to the following hydraulic jump types: BJ refers to a B-Jump, UJ represents an Undular Jump, PSJ denotes a Periodic Submerged Jump, and SSJ indicates a Tall End Sill Jump. These jump types are explained in detail in Fig. 4, which is presented later in the document.

3. Results

3.1. Effect of the ISB geometry on the flow pattern and basis for ISB flow classification

When a drop and an enlargement are combined, the jump types are influenced by both enlargement and drop. Fully 3D and complex overlapping and mutual effects of enlargement and drop have also been detected on flow field structures, whereas the individual presence of each of these measures (enlargement and drop) has not been detected [12]. However, in a typical ISB geometry, owing to a positive step at the ISBs downstream, the jump types are preferable to those detected in only drop cases and not in an enlargement, particularly when the ISB length is relatively short. The classification of the different hydraulic jumps observed in the present research is shown in Figs. 4 and 5.

The B-jump (BJ) occurs when there is no end sill, featuring a non-submerged nappe plunging into the ISB with weak horizontal circulation and supercritical surface flow. The Undulated Jump (UJ) emerges with a taller end sill, characterized by symmetric V-shaped waves and steady rollers due to the interaction between subcritical upstream flow and supercritical outflow. A shorter end sill disrupts the BJ, creating an Asymmetric Spatial Jump (ASJ) with 3D, asymmetric eddies and an oblique spindle-like flow. Moderate end sill heights and medium ISB depths produce a periodic submerged jump (PSJ), distinguished by periodic and less stable submerged flow. Conversely, taller end sills or deeper ISBs result in a steady submerged jump (SSJ) with stable, symmetric, and steady submerged behavior, representing the most compact and efficient energy dissipation.

When there is no end sill at the ISB downstream (Figs. 4a and b and 5a), the flow plunges into the ISB in the form of a nappe flow, whereas underneath, the nappe merges into the stagnant water within the ISB. Conversely, the surface of the nappe is still exposed to the air and is completely visible. Therefore, air was entrained into the water at the lateral side of the nappe, and minor jumps were created in two parallel lines. After plunging into the ISB, the nappe flow expanded rapidly, widening the surface roller until it occupied the whole channel width. The surface flow in the ISB is supercritical in this type of jump. If the ISB is relatively shallow (smaller drop number), this condition is more likely to be observed. However, weak horizontal circulations are formed due to the relatively small expansion ratio of the ISB ($k = 0.2$) at the lateral sides of the ISB. The area upstream of the jump toe (plunging point) was stagnant, with a minor contribution to the main flow near the nappe sides. This type of jump is known as a B-jump (BJ) (Fig. 5a), in which a nonsubmerged nappe plunges into the ISB.

As a taller end sill is mounted at the ISB downstream end, the subcritical flow gradually moves upstream and submerges the supercritical outflow of the bottom outlet. The spindle-plunging jet disappears into the ISB. In this case, a narrow and symmetric supercritical current was observed along the centerline of the ISB and created V-shaped steady waves at the water's surface, in which the rollers' front was

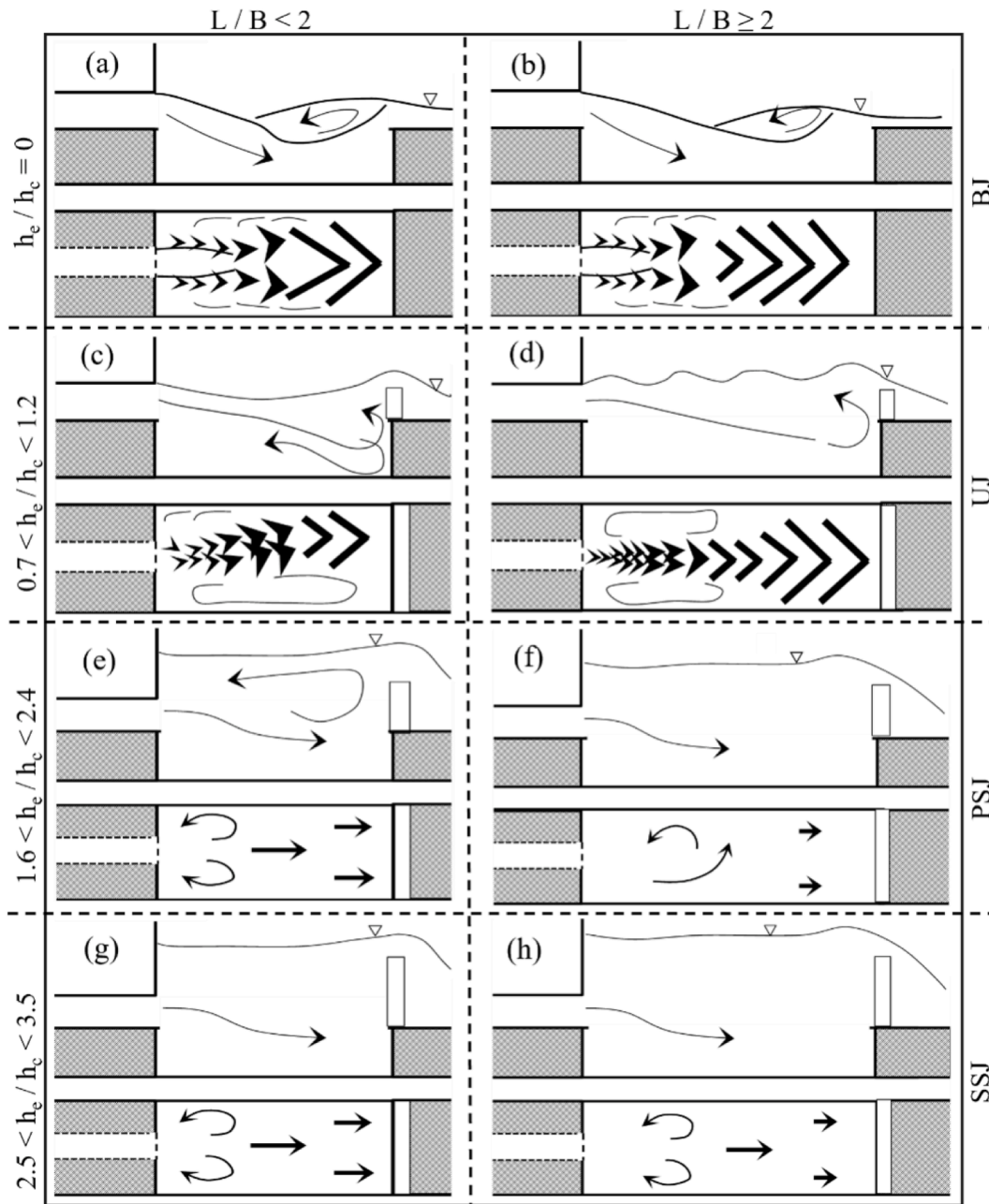


Fig. 4. The effects of the ISB length and end sill height on the schematic view of jump types.

continuously converging and diverging, creating several quadrilaterals. This dissipative phenomenon, an undulated jump (UJ), occurs when two symmetric eddies of nearly equal size form on either side of the central supercritical current. This behavior is influenced by the interaction between the upstream subcritical flow and the supercritical outflow downstream of the bottom outlet. A schematic representation of this jump type is shown in Figs. 4d and 5b.

For shorter end sill heights ($0.7 < h_e/h_c < 1.2$), the end sill forces the jump to be confined in the beginning part of the ISB. A short-end sill increases the sequent depth, resulting in subcritical flow near one sidewall that breaks the front of the BJ. Then, the subcritical flow moves toward the opposite wall and forms a large horizontal eddy. Because of the three-dimensional characteristics of this type of jump and its asymmetric nature, it is called an asymmetric spatial jump (ASJ) (Fig. 4c). The top view of the jump is similar to an oriented 'spindle', whose longitudinal axis is not straight along the channel but oblique.

Thus, the break of the front in the BJ, caused by a short end sill, originates at the ASJ. This type of jump is more likely to occur in the case of relatively short-end sill heights and shallow ISBs (small drop numbers).

If there is a wall above the bottom outlet, a further increase in the end sill height leads to the submergence of the bottom outlet. The wall above the bottom outlet prevents the jump from moving into the upstream approach channel. The submerged jumps observed in the present research were mostly periodic and steady submerged jumps. The medium height of the end sill mainly provides the PSJ (Fig. 4f). However, the combination of deep ISBs with a medium height of the end sill could successfully form a steady submerged jump (SSJ).

A short ISB length ($L/B < 2$) combined with a medium end sill height (Fig. 4e) established a steady and symmetric flow referred to as a steady submerged jump. The longer one ($L/B > 2$) was found to result in a more unstable and periodic flow, and it was named the periodic submerged jump (PSJ) (Figs. 4f and 5c). A shorter ISB with a medium height of the

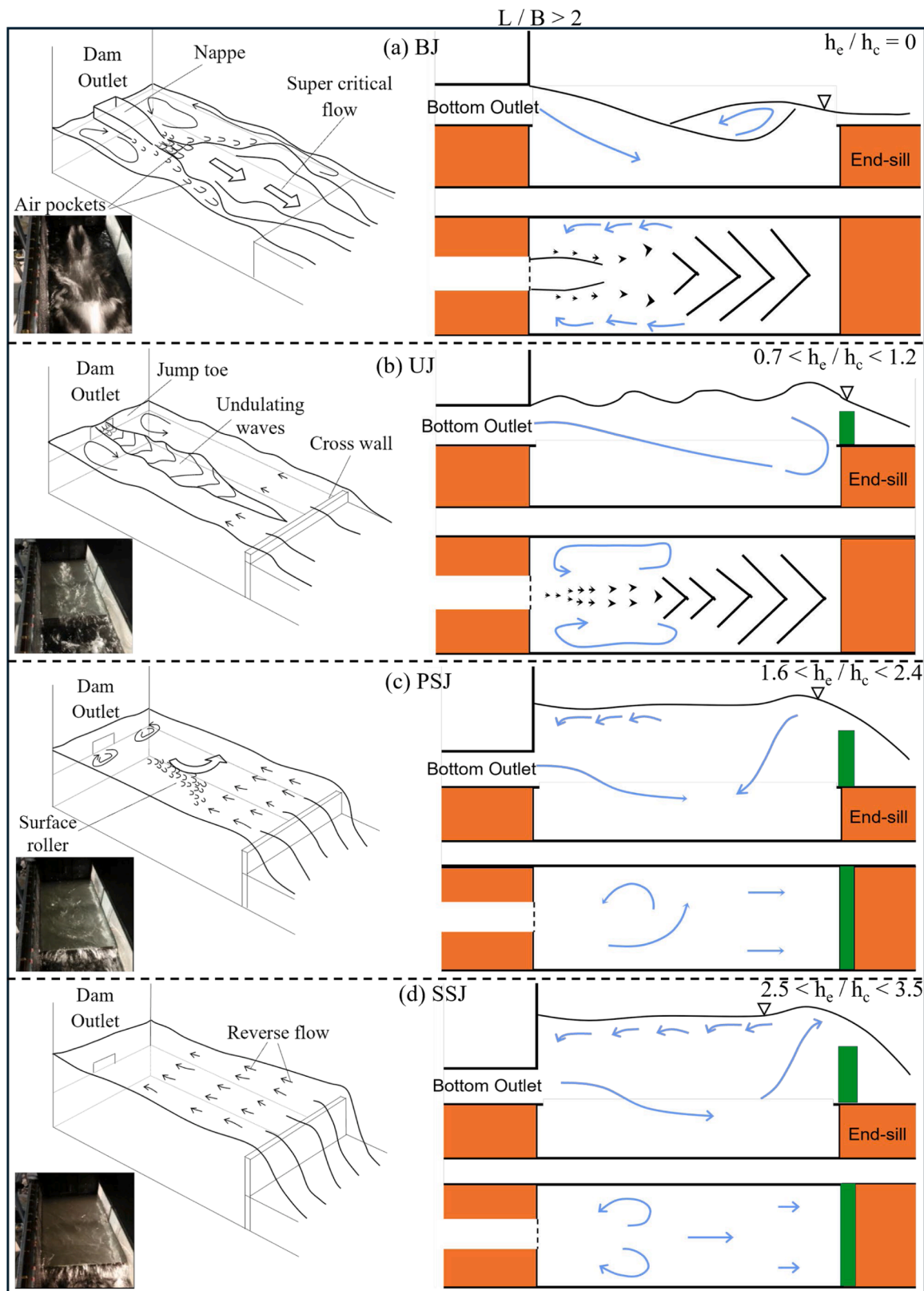


Fig. 5. Schematic detail view of the jump types ($L/B > 2$): a) B-jumps (BJ), b) U-jumps (UJ), c) periodic submerged jumps (PSJ), and d) steady submerged jumps (SSJ).

end sill may be an optimum case from the perspective of jump stability and compactness. A tall end sill ($2.5 < h_e/h_c < 3.5$), independent of the ISB depth or ISB length, always initiates a steady submerged jump. This type of jump is characterized by its stability and symmetry (Figs. 4g and 4h and 5d).

3.2. Analysis of nondimensional geometric governing parameters and their effects on flow field characteristics

The effects of various non-dimensional geometric parameters, such as the normalized ISB length (L/B), normalized drop number ($S = s/h_1$), normalized end sill height $(s + h_e)/h_1$, and degree of end sill width $(1 - (b_e/B))$, on velocity reduction, subsequent depth, and submergence depth are investigated.

The height of the end sill plays a significant role in determining the type of hydraulic jump formed. Shorter end sills typically lead to confined jumps, whereas taller end sills promote steady submerged jumps that facilitate better energy dissipation [52]. Table 3 defines each abbreviation used in this study and its relevant values.

3.3. The effect of the normalized ISB length

Table 4 lists the selected test cases used to investigate the influence of the normalized ISB length on the ISB performance, summarizing the governing nondimensional and dimensional parameters in these tests. Fig. 6a–c show the effects of changes in the normalized ISB length on the normalized longitudinal velocity reduction within an ISB, normalized submergence depth at the face of the bottom outlet, and normalized water head above the end sill, respectively. These figures visualize these effects for different combinations of end sill height and ISB depth at a given $Fr = 4.3$.

In this table, (X)SM refers to a configuration with a shallow drop height ($s/h_1 = 1$) and medium-end sill height ($h_e/h_c = 0.9$), whereas (X)SD represents a configuration with a deep drop height ($s/h_1 = 1.5$) and medium end sill height ($h_e/h_c = 0.9$). The (X)MM configuration is characterized by a shallow drop height ($s/h_1 = 1$) and moderate end sill height ($h_e/h_c = 1.8$), whereas (X)MD corresponds to a deep drop height ($s/h_1 = 1.5$) and moderate end sill height ($h_e/h_c = 1.8$). XTM describes a configuration with a shallow drop height ($s/h_1 = 1$) and tall end sill height ($h_e/h_c = 2.7$), whereas (X)TD is a configuration with a deep drop height ($s/h_1 = 1.5$) and tall end sill height ($h_e/h_c = 2.7$). In these notations, S, M, and L refer to the short, medium, and long normalized ISB lengths (L/B) used to classify the test cases.

Table 3 Definitions of the formulations used in the present research for the naming system for each test case.

Abbreviation	Meaning	Example	Relevant values		
			ISB length	ISB end-sill height	ISB depth
S	Short, Shallow, Small	A short ISB length, a small end-sill height, a shallow ISB depth	75 cm	4 cm	5 cm
M	Medium	A medium ISB length, a medium end-sill height, a medium ISB depth	100 cm	8 cm	10 cm
D	Deep	A deep ISB depth	-	-	15 cm
T	Tall	A tall end-sill height	-	12 cm	-
T'	A very tall	A very tall end-sill height	-	13.5 cm	-
N	Nothing (without)	No end-sill	-	0 cm	-
L	Long	A long ISB length	125 cm	-	-

In Fig. 6a, U_0 is the flow velocity at the face of the bottom outlet at section I, and U_2 is the maximum recorded velocity just upstream of the end sill (at section II, located at the center of the cross-section). Fig. 6 shows that the ISB performance concerning velocity reduction (of the plunging jet) is enhanced by increasing the ISB length. The velocity reduction appears to be the smallest in ISBs with short-end sill heights ($h_e/h_c = 0.9$) and deep drops ($s/h_1 = 1.5$). Combining the short-end sill ($h_e/h_c = 0.9$) with a medium drop height ($s/h_1 = 1$) resulted in a greater velocity reduction. This is because, in an ISB with a medium drop height, a larger portion of the incoming plunging jet hits the bottom of the ISB than in deeper ISBs, resulting in more dissipation of the jet's energy. The highest jet velocity reduction is observed in the presence of a tall end sill ($h_e/h_c = 2.7$) combined with medium to deep drops ($s/h_1 = 1$ and 1.5). A tall end sill suppresses the incoming jet by fully submerging it. A medium to deep ISB provides enough room for the flow to develop and recirculate in a 3D form within the ISB. These two effects cause dissipation of the incoming jet velocity. Therefore, we can reduce the ISB length by considering a taller end sill. A reduction in the ISB length is cost-efficient. Considering the economic aspects of design, a medium normalized ISB length equal to 2 ($L/B = 2$) may be the maximum value.

The submergence depth decreases with increasing normalized ISB length. Increasing the ISB length allows more space for plunging jets into the ISB. Then, the jump becomes less compacted by the subsequent depth, consequently decreasing the submergence depth. Fig. 6a and b reveal that a medium end-sill height ($h_e/h_c = 1.8$) combined with a medium drop number ($s/h_1 = 1$) resulted in an optimum performance: relatively high flow velocity reduction and low submergence depth.

Fig. 6c shows the normalized water depth above the end sill versus the normalized ISB length. This figure reveals why test case (X)TM performed best at a medium ISB length. The MTM (medium-to-all medium) test case provides a greater normalized water depth and a medium submergence depth above the end sill. The experimental results show that a medium ISB length can perform optimally if the other parameters are selected properly. Therefore, the total costs of projects can be reduced considerably.

3.4. The effect of the decrease in the drop number

The drop number is one of the main parameters that should be selected carefully, as its optimum value can provide many advantages for an ISB construction project. An incorrect value for this parameter is expensive for the project and environment. An optimum value for the drop number saves money through decay because digging out the ground is necessary. Additionally, the optimum ISB depth can increase the energy dissipation of the plunging jet into the ISB. Moreover, an acceptable depth of ISB is needed to create a pool below FMD and a suitable habitat structure for aquatic animals should be proposed. Table 5 shows the test configuration used to determine the effect of the number of ISB drops.

In this table, the MS(X) configuration features a shallow end sill height ($h_e/h_c = 0.9$) with varying drop numbers ($s/h_1 = 1, 2, 3$), where S, M, and D represent short ($s/h_1 = 1$), medium ($s/h_1 = 2$), and deep ($s/h_1 = 3$) drop numbers, respectively. The MM(X) configuration involves a moderate end sill height ($h_e/h_c = 1.8$) with the same varying drop numbers, and MT(X) represents a configuration with a tall end sill height ($h_e/h_c = 2.7$) and varying drop numbers. These configurations allow the analysis of the impact of the drop number on the velocity reduction, submergence depth, and water column height above the end sill, thereby contributing to a better understanding of the ISB performance under different drop conditions.

Based on the classification of Ohtsu and Yasuda [14] drop types, the drop numbers in this study are known as low drops, $0.5 \sim 1.5 \leq s/h_1 \leq 8 \sim 9$. Fig. 7a depicts the normalized velocity versus the normalized ISB length (L/B) for different drop numbers. The horizontal axis in this figure represents the drop number, and the vertical axis represents the normalized velocity. The ISB performance exhibited two different

Table 5
The test configuration aimed to reveal the effect of the drop number on the ISB performance.

Case	Q (l/s)	Fr ₁	h ₁ (cm)	b ₁ (cm)	L (cm)	s (cm)	h _e (cm)	b _e (cm)	h _e /h _c	s/h ₁
MS(X)	S	15	4.3	5	100	5	4	50	0.9	1
	M	15	4.3	5	100	10	4	50	0.9	2
	D	15	4.3	5	100	15	4	50	0.9	3
MM(X)	S	15	4.3	5	100	5	8	50	1.8	1
	M	15	4.3	5	100	10	8	50	1.8	2
	D	15	4.3	5	100	15	8	50	1.8	3
MT(X)	S	15	4.3	5	100	5	12	50	2.7	1
	M	15	4.3	5	100	10	12	50	2.7	2
	D	15	4.3	5	100	15	12	50	2.7	3

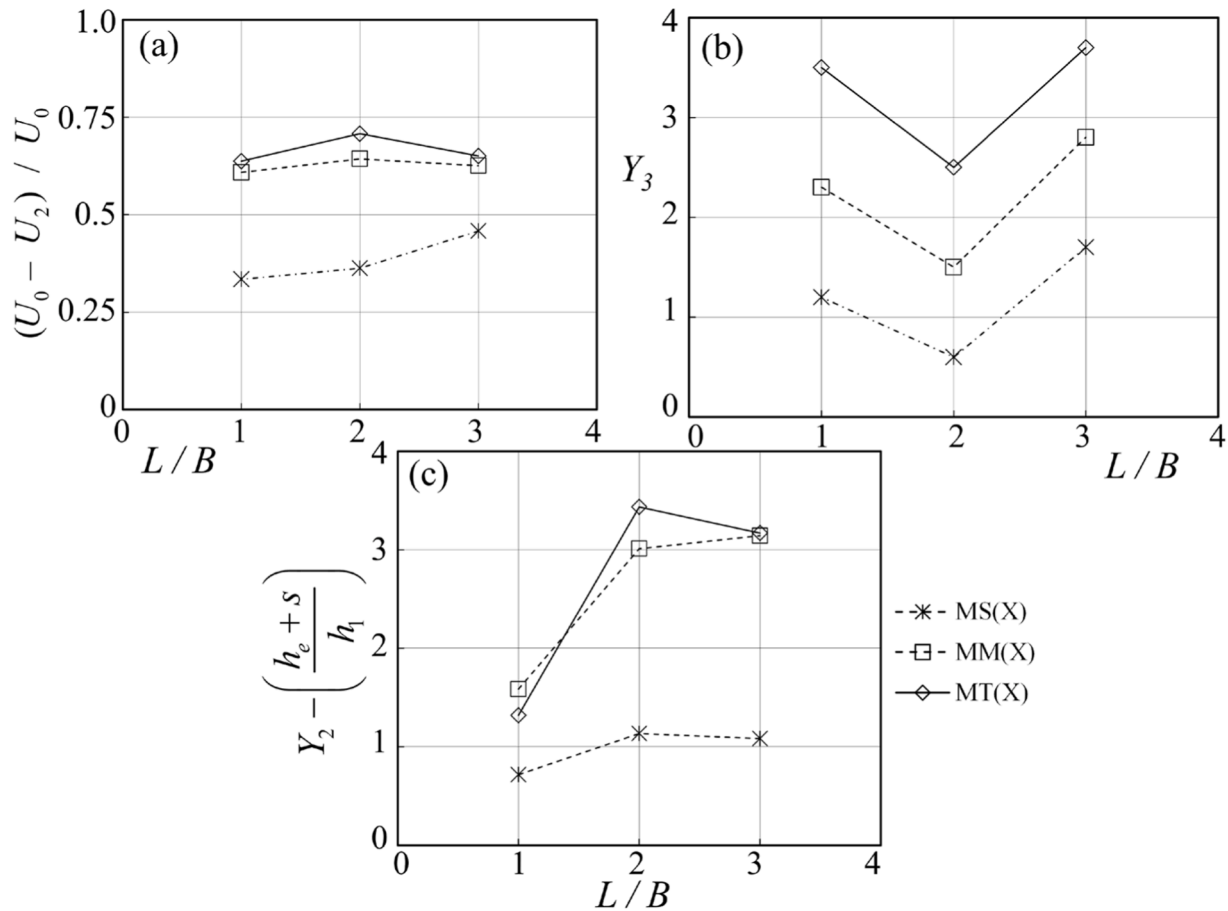


Fig. 7. Influence of drop number (s/h_1) on ISB performance for different end sill heights: (a) normalized velocity ($\frac{U_0 - U_2}{U_0}$) versus the normalized ISB length (L/B), illustrating trends for shorter (MS(X)) and taller end sills (MM(X), MT(X)) (b) submergence depth versus drop number for a medium ISB length (100 cm) and a constant Froude number ($Fr = 4.3$), highlighting the relationship between submergence depth and ISB performance; (c) normalized water head above the end sill versus drop number.

normalized water head above the end sill increased (Fig. 7c). Moreover, a further increase in the drop number did not lead to a greater water column above the end sill, as shown in Fig. 7c. The velocity profiles along the centerline of the ISB and in the streamwise flow direction are shown in Fig. 8.

3.5. Effect of the normalized end sill height

Another important geometrical parameter that should be selected carefully is the end sill height. The test configuration is shown in Table 6, which presents the designated experimental tests. Four tests were designed to identify the effect of the end sill height on the ISB performance; all the parameters were constant, and only the end sill height varied.

In this table, "M(X)" indicates the general category of test cases, where "M" stands for medium, "S" represents short, and "D" denotes deep drop heights. Specifically, the configurations M(X)S, M(X)M, and M(X)D are used to categorize the experiments into short, medium, and deep drop heights, with the respective end sill heights varying accordingly (from none to tall). The "T" and "T'" tests represent cases with taller and very tall end sill heights. The experiments without any end sill (e.g., MND or MNS) showed minimal normalized velocity reduction of approximately 25%. In contrast, the cases with taller end sills (e.g., M, T, T') achieved significant reductions in velocity, up to 60%. However, increasing the height from tall (T) to very tall (T') did not significantly improve the ISB performance, highlighting that an optimal end sill height, typically greater than 2, maximizes the velocity reduction without further improvement from excessively tall sills.

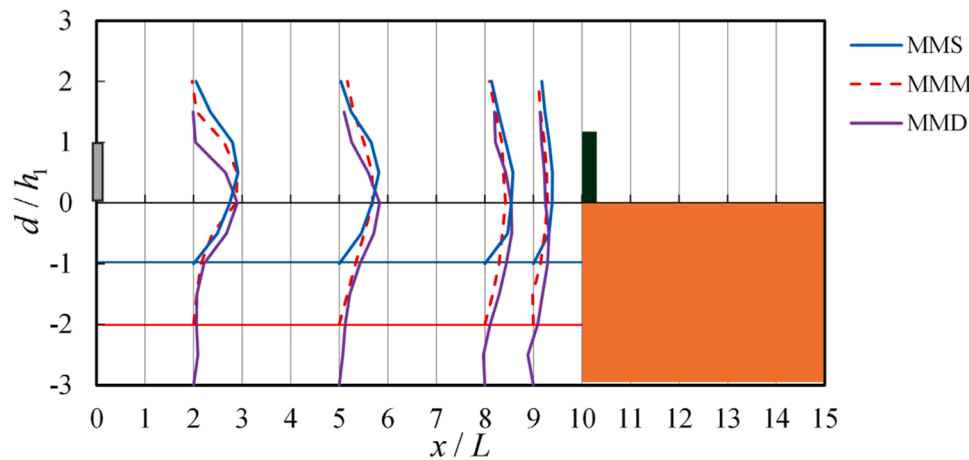


Fig. 8. Velocity profiles along the centerline of the ISB in the streamwise flow direction for different drop numbers (s/h_1) and end sill heights. The profiles correspond to three cases: MMS (medium end-sill height with short drop number), MMM (medium end-sill height with medium drop number), and MMD (medium end-sill height with tall drop number).

Table 6

The test configuration aims to identify the influence of the relative end sill height on the ISB performance.

Case		Q (l/s)	Fr ₁	h ₁ (cm)	b ₁ (cm)	L (cm)	s (cm)	h _e (cm)	b _e (cm)	h _e /h _c	s/h ₁
M(X)S	N	15	4.3	5	10	100	5	0	50	0	1
	S	15	4.3	5	10	100	5	4	50	0.9	1
	M	15	4.3	5	10	100	5	8	50	1.8	1
	T	15	4.3	5	10	100	5	12	50	2.7	1
	T'	15	4.3	5	10	100	5	13.5	50	3	1
M(X)M	N	15	4.3	5	10	100	10	0	50	0	2
	S	15	4.3	5	10	100	10	4	50	0.9	2
	M	15	4.3	5	10	100	10	8	50	1.8	2
	T	15	4.3	5	10	100	10	12	50	2.7	2
	T'	15	4.3	5	10	100	10	13.5	50	3	2
M(X)D	N	15	4.3	5	10	100	15	0	50	0	3
	S	15	4.3	5	10	100	15	4	50	0.9	3
	M	15	4.3	5	10	100	15	8	50	1.8	3
	T	15	4.3	5	10	100	15	12	50	2.7	3
	T'	15	4.3	5	10	100	15	13.5	50	3	3

In the case of experiments without an end sill (e.g., MND or MNS), the normalized velocity remained very low, approximately 25 %; even increasing the ISB depth could not considerably improve the ISB performance (Fig. 9a). However, in the cases with a taller end sill (M, T, and T'), the magnitude of the normalized velocity increased to 60 % of the initial velocity. However, this finding indicates that increasing the height of the end sill from T to T' (from tall to very tall) did not enhance the performance of the ISB in terms of normalized velocity. Thus, it can be concluded that a taller end sill could dissipate more energy than a shorter end sill. However, increasing the end sill height above the optimum value did not enhance the performance of the ISB. A normalized end sill height, h_e/h_c greater than 2, may provide an acceptable velocity reduction of approximately 60 to 70 % within the ISB.

Fig. 9b shows the variation in the submergence depth against the normalized end sill height. Three similar data points are plotted in this figure related to those cases with given ISB lengths but different ISB depths. Fig. 9c depicts the relationship between the normalized water column above the end sill and the normalized height. Fig. 10a also shows the streamwise velocity profile along the centerline of the ISB at different end sill heights, N, M, and T.

Fig. 10b and c show the transverse velocity profiles of the submerged jump, where at the last section in the ISB, section II is located just upstream of the end sill for the MMM and MTM, respectively. A comparison of these two figures reveals that a taller end sill could break the jump front and reduce the maximum velocity of the jump front by almost 30 % more than in the case with a medium end sill height.

Moreover, in the case of taller end-sills, the reverse flow intensified more than in cases with shorter end-sills. A taller end sill may also reduce the symmetry of the jump front rather than the medium end sill height. In the case of MTM, the jump front is asymmetric and oblique to the right wall of the channel.

This observed asymmetry in the jump front with taller end sills is significant, as it can influence the overall efficiency of the ISB in terms of energy dissipation and sediment transport. This asymmetry may lead to localized flow phenomena that could result in uneven sediment deposition or erosion within the ISB, affecting its long-term stability and performance. Furthermore, the increased reverse flow and velocity reduction observed in taller end sill configurations suggest that such designs may be particularly effective in applications requiring high energy dissipation, such as flood control, or when designing stilling basins with significant discharge volumes. However, changes in flow symmetry should be carefully considered to avoid potential drawbacks in other aspects of ISB operation, such as sediment clogging or increased maintenance requirements.

3.6. Effect of the relative end sill width

To clarify the effect of free space (end sill width) on the velocity reduction along the ISB, two groups of tests were designed, in which all the parameters were held constant and only the end sill width varied. The first group of experiments focused on the effects of free spaces on the performance of ISBs equipped with medium-end sill heights (MMMs),

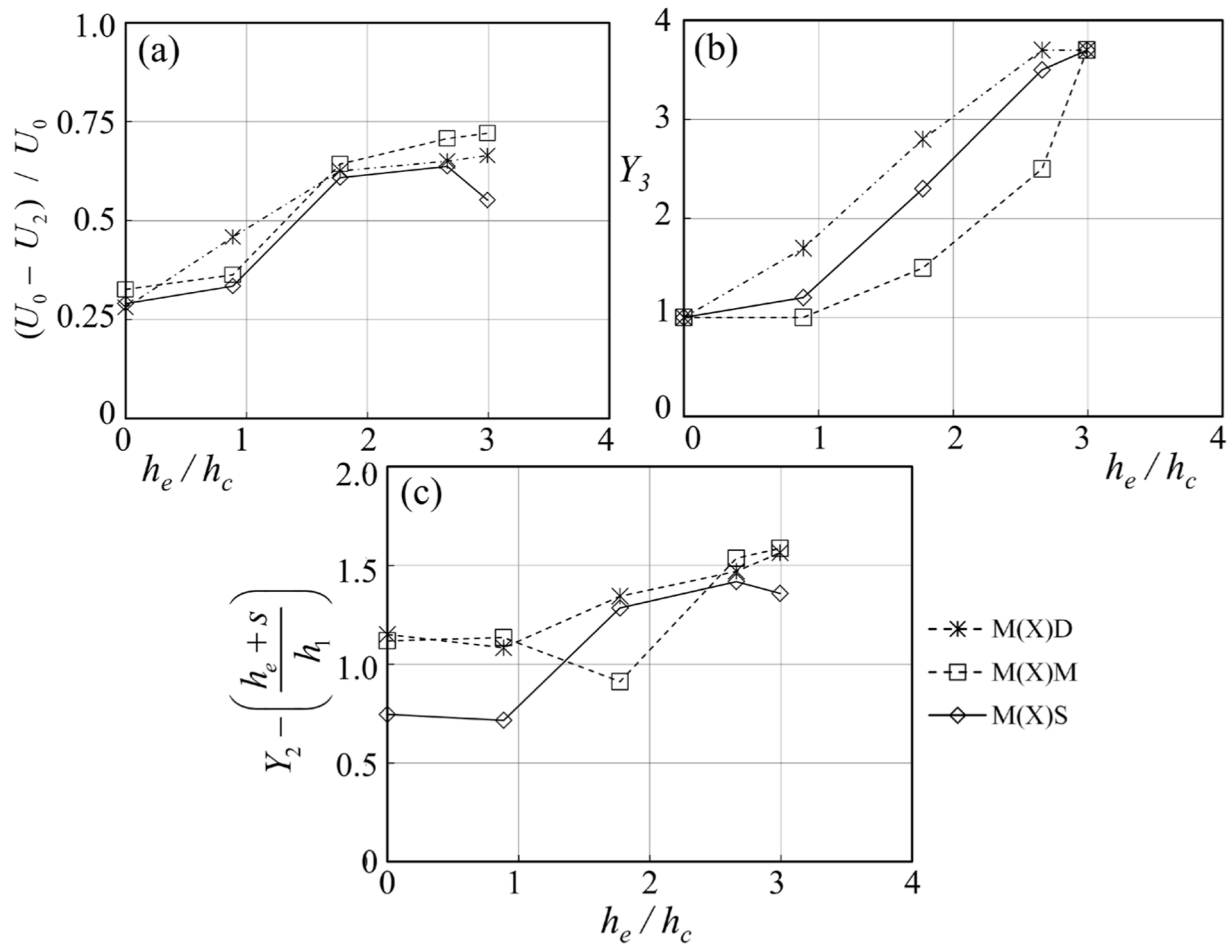


Fig. 9. (a) Normalized velocity versus end sill height (h_e/h_c) for varying ISB depths ($Fr = 4.3$). (b) Submergence depth (S/h_1) versus h_e/h_c for different end sill heights and ISB depths. (c) Normalized water column height versus h_e/h_c . The figure includes three cases: M(X)D (medium end-sill height with tall drop number), M(X)M (medium end-sill height with medium drop number), and M(X)S (medium end-sill height with short drop number).

and the second group focused on those equipped with taller end sill heights (MTMs). The test configurations designed for this section are tabulated in Table 7. It is necessary to explain the formulation that is used in this table. For example, the MMM has already defined a geometry of ISBs in which the ISB length, end sill height, and ISB depth are all intermediate, and their values are 100 cm, 8 cm, and 10 cm, respectively. In test cases such as MMM-2f, all the variables are the same as those in the case of the MMM, and only the width of the end sill is reduced. “f” is the abbreviation for free space. “2f” indicates two free spaces at both sides of the end sill. Each “f” is equal to 5 cm. For example, “2f” indicates that the total width of the end sill is 10 cm less than the width of channel B, and 4f indicates two free spaces, each of which is 10 cm.

In Table 7, MMM refers to the geometry of the ISB with a medium end sill height (8 cm), medium ISB depth (10 cm), and medium ISB length (100 cm). “2f” denotes the configuration where the end sill width is reduced by 10 cm, with “f” representing a 5 cm free space on each side of the end sill. The MTM refers to the ISB configuration with a taller end sill height (12 cm), medium ISB depth (10 cm), and medium ISB length (100 cm). Similarly, “2f” in the MTM test cases reduced the end sill width to 10 cm because of the free space on both sides of the end sill.

Fig. 11a shows the variation in the normalized velocity reduction with the normalized free space width. Considering that two free spaces on both sides of the end sill slightly reduced the performance of the ISB for velocity reduction. However, the general trend of the plotted curves reveals that selecting a taller end sill with free space may provide better velocity reduction performance than selecting a full end sill with no free

space. Thus, a taller end sill could offer better ISB performance in addition to facilitating fish and sediment passage.

The relationship between the submergence depth and the end sill width is plotted in Fig. 11b. Decreasing the end sill width resulted in a reduction in the submergence depth. The total trend observed in this figure agrees with previous figures on velocity reduction and subsequent depth. Fig. 11c shows the variation in the normalized water head above the end sill versus the degree of end sill over width for two families of end sill heights M and T (medium and tall), a given medium ISB length and a constant Froude number ($Fr = 4.3$). The overall trend for the variation in the normalized water head above the end sill is inconsistent with the velocity reduction in Fig. 11a.

Fig. 12 presents the transverse velocity profiles upstream of the end sill, aligned with the bottom outlet’s lower invert. These profiles illustrate the effects of varying the width of the free space in the end sill on the flow characteristics. The results highlight that changes in the end sill width significantly influence the velocity distribution across the basin width, affecting the uniformity and magnitude of velocities. A more uniform velocity distribution upstream of the end sill promotes effective energy dissipation by reducing localized high-velocity zones and enhancing flow stabilization, which is critical for the efficient hydraulic performance of the stilling basin. Optimizing the end sill geometry also contributes to minimizing turbulence downstream, ensuring improved structural stability and reducing wear and erosion risks. These findings underscore the importance of end sill design as a key parameter in achieving the dual goals of energy dissipation and flow control.

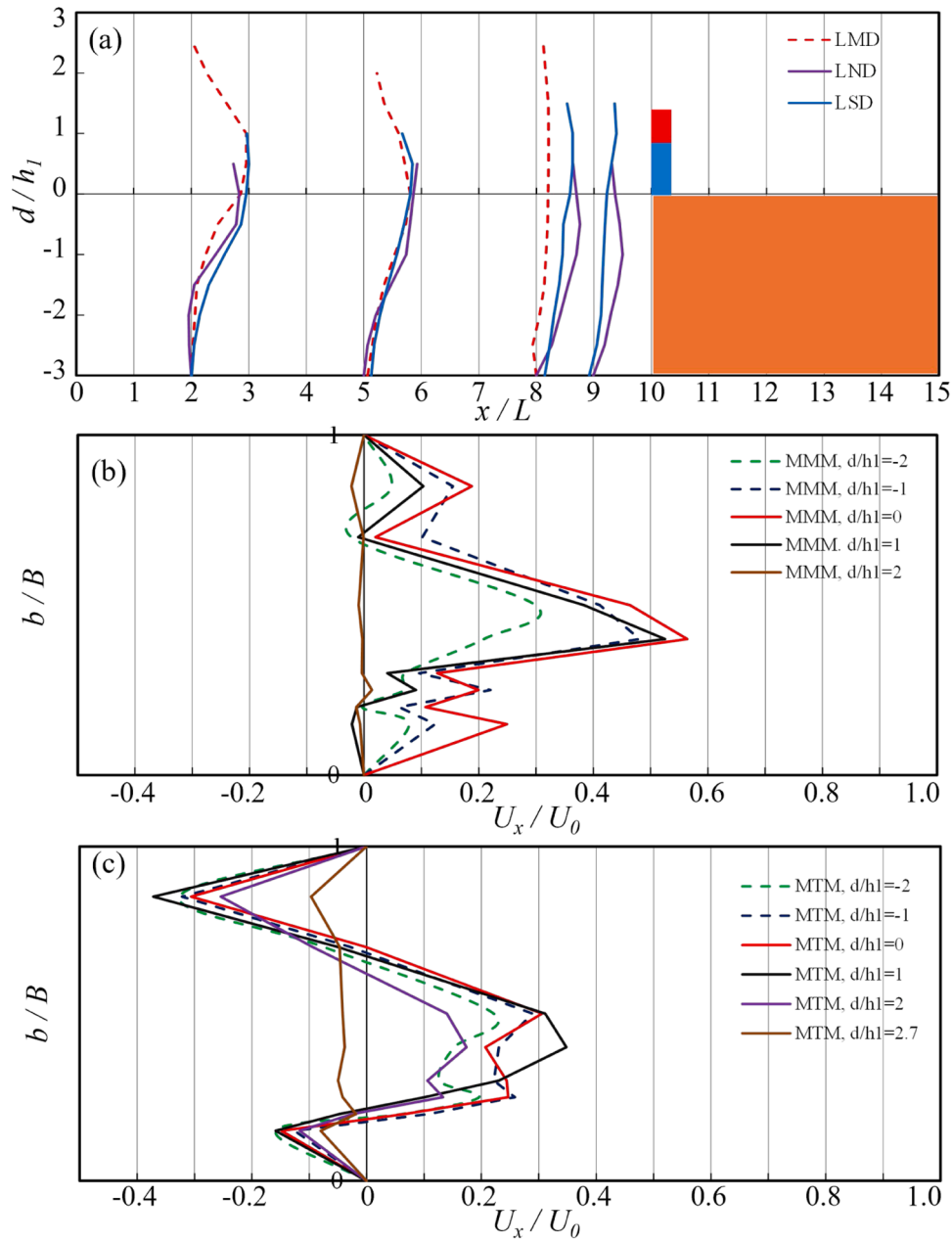


Fig. 10. (a) Streamwise velocity profile along the ISBs for various end sill heights in the presence of long ISBs, deep ISBs, and constant Froude numbers ($Fr = 4.3$). (b)–(c) Transversal velocity profile just upstream of the end sill at different normalized depths from the lower invert of the bottom outlet; (b) $h_e/h_c = 1.7$, $s/h_1 = 2$, and $Fr = 4.3$; (c) $h_e/h_c = 2.8$, $s/h_1 = 2$, and $Fr = 4.3$.

Table 7

The test configuration aims to clarify the effect of the degree of end sill width on the ISB performance.

Case	Q (l/s)	Fr_1	h_1 (cm)	b_1 (cm)	L (cm)	s (cm)	h_e (cm)	b_e (cm)	h_e/h_c	s/h_1	
MMM	-	15	4.3	5	10	100	10	8	50	1.8	2
	-2f	15	4.3	5	10	100	10	8	40	1.8	2
	-4f	15	4.3	5	10	100	10	8	30	1.8	2
	-6f	15	4.3	5	10	100	10	8	20	1.8	2
MTM	-	15	4.3	5	10	100	10	12	50	2.7	2
	-2f	15	4.3	5	10	100	10	12	40	2.7	2
	-4f	15	4.3	5	10	100	10	12	30	2.7	2
	-6f	15	4.3	5	10	100	10	12	20	2.7	2

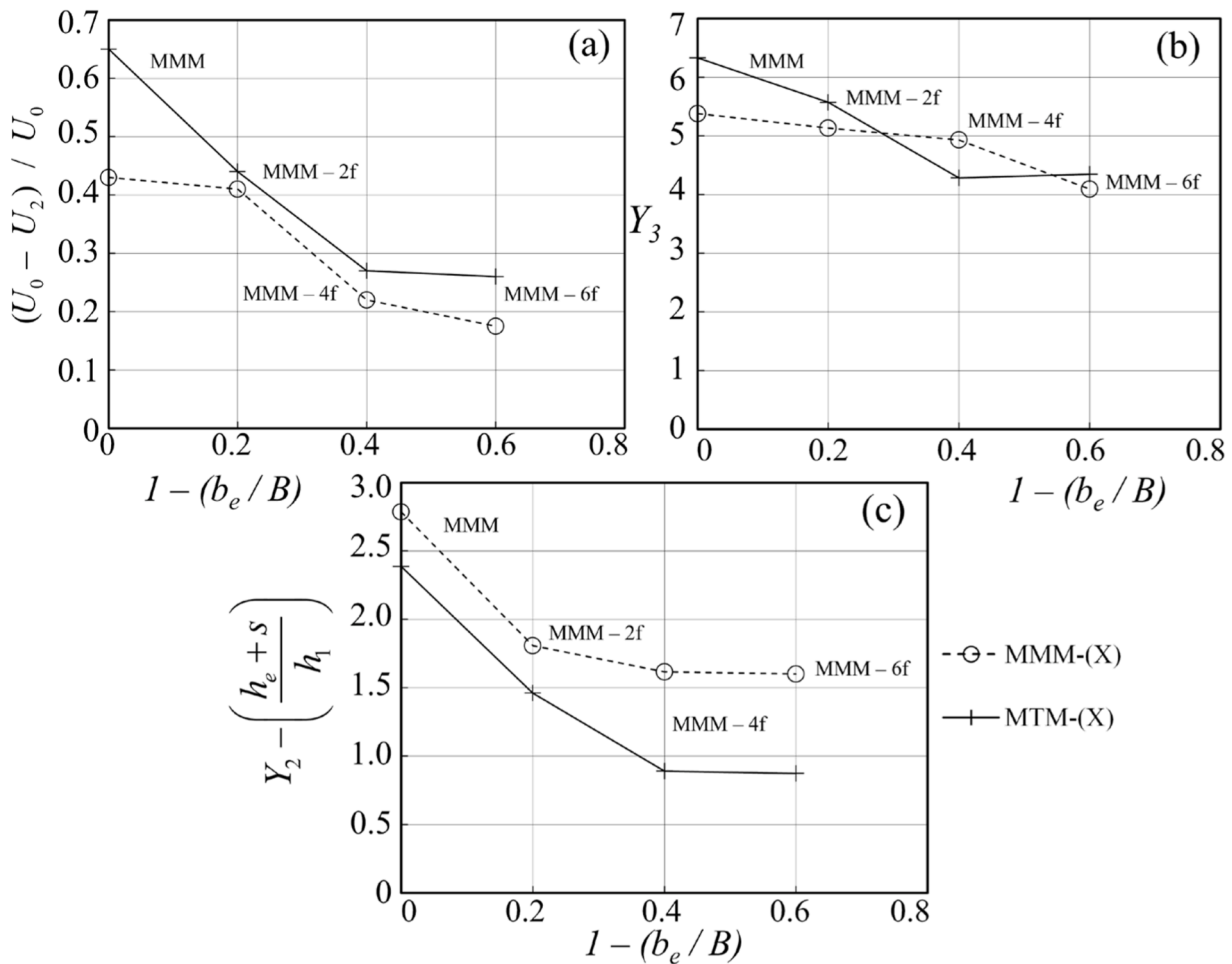


Fig. 11. (a) Variation in the normalized velocity reduction along the ISB, (b) submergence depth versus the degree of end sill width, and (c) normalized water head above the end sill versus the degree of end sill width for different end sill heights, medium ISB lengths, and a constant Froude number ($Fr = 4.3$).

3.7. Flow conditions downstream of the ISBs

Fig. 13 shows the normalized velocity reduction between sections I and IIV (downstream of the ISB). U_5 is the average velocity of flow at section IIV. The overall trend of the data plotted in this figure shows that the normalized velocity reduction is reduced by increasing the normalized height of the end sill.

In other words, contrary to the necessity of taller end-sills to create a steady submerged jump within a confined space, taller end-sills negatively reproduce the higher flow velocities at the ISBs downstream. A medium-height end sill can guarantee better conditions for the flow field downstream of the ISB. The green box in Fig. 13 shows the optimum range for the normalized end sill height. Thus, in the case of submerged jumps within the ISB, the best-normalized end sill height, h_e/h_c , for creating acceptable downstream conditions ranged from 2–3.

4. Discussion

The construction of flood mitigation dams on river systems is becoming increasingly popular and vital for the near future. This is particularly true in arid or semiarid countries such as Iran, Saudi Arabia, and Yamane, which suffer from frequent flash floods. Moreover, in Japan, flood mitigation dams should be eco-friendly and secure the continuity of sediment and fish transportation in addition to flood control purposes. In countries located in arid and semiarid areas, flash floods mostly occur in seasonal rivers, in which the environmental aspects are less important. A stilling basin downstream of a flood

mitigation dam plays a key role in this structure, not only because of energy dissipation but also because it ensures the continuity of the sediment supply downstream and fish migration upstream. The combined effects of key parameters on the flow pattern and flow dissipation processes within a stilling basin were examined in this study.

4.1. Influences of drop height, ISB length, and end sill geometry on hydraulic jump types

The experimental results demonstrate that the interaction between the drop height, ISB length, and end sill geometry significantly influences the flow patterns and hydraulic jump behavior within in-ground laying basins (ISBs) (Figs. 4, 5, 9–13 and Tables 3–7). Various configurations of these parameters lead to distinct hydraulic jump types. Without an end sill, the B-jump (BJ) forms, characterized by a non-submerged nappe flow that results in a less stable hydraulic jump. As the end sill height increases, an undulated jump (UJ) emerges, characterized by symmetric V-shaped waves. This jump is more pronounced with taller end sills, indicating that a taller sill contributes to more stable flow dynamics. Conversely, short-end sills generate an Asymmetric Spatial Jump (ASJ), dominated by oblique, spindle-shaped eddies that are less stable. Additionally, submerged jumps can be either periodic (PSJ) or steady (SSJ), with the SSJ offering the most consistent and efficient energy dissipation. The significance of these findings lies in understanding the relationship between the end sill height and hydraulic jump type, which allows engineers to optimize energy dissipation and flow stability in ISB design, enhancing the overall system efficiency.

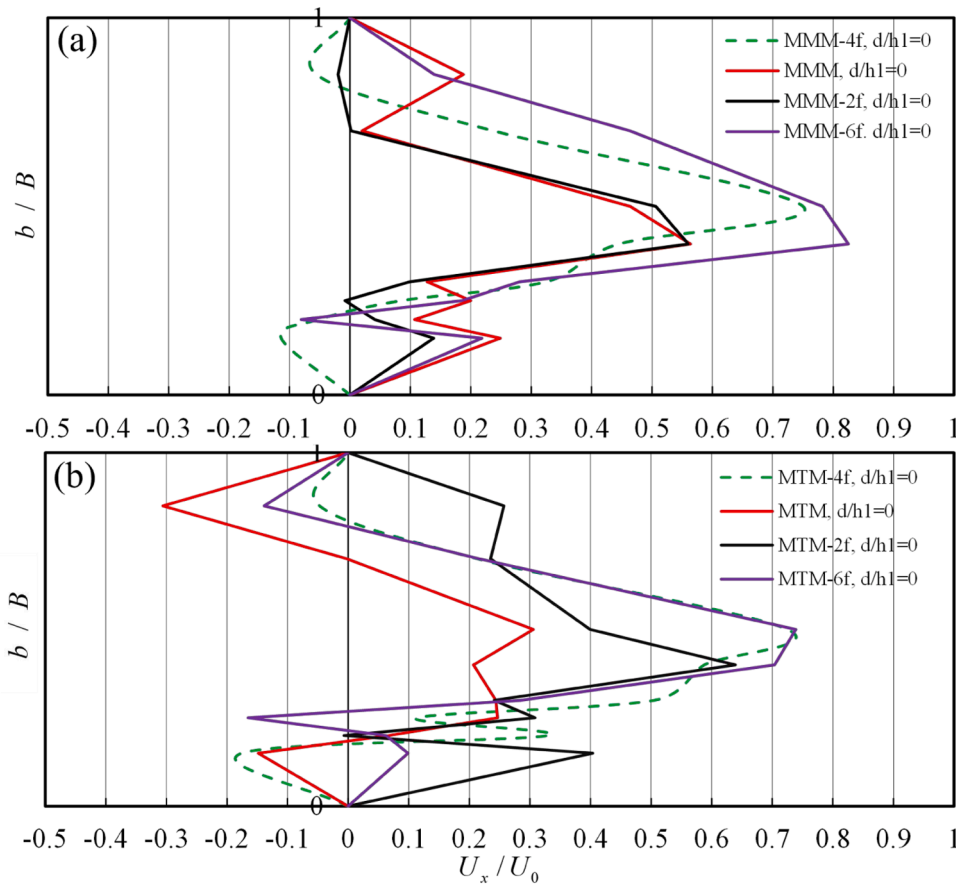


Fig. 12. Transversal velocity profile just upstream of the end sill for different end-sill widths where leveled with the lower invert of the bottom outlet: (a) $d/h_1 = 0$, $h_e/h_c = 1.7$, $s/h_1 = 2$, and $Fr = 4.3$; (b) $d/h_1 = 0$, $h_e/h_c = 2.8$, $s/h_1 = 2$, and $Fr = 4.3$.

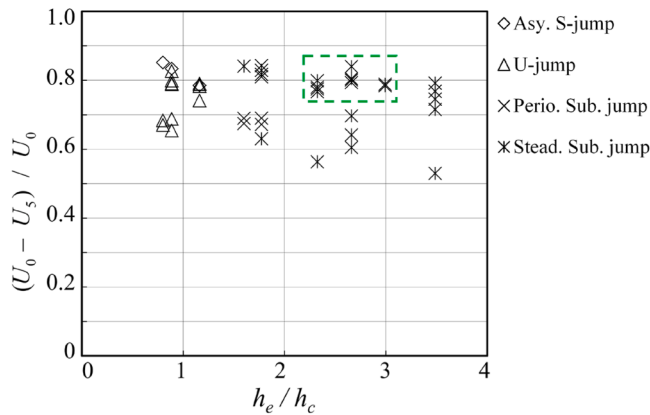


Fig. 13. Velocity reduction between sections I and IIV influenced by different normalized end sill heights.

4.2. Impact of ISB geometry on the stability and energy dissipation

This study highlights that shorter ISBs combined with medium-end sill heights tend to favor steady submerged jumps, balancing stability, and compactness (Figs. 4–8, and Tables 3 and 5). This configuration promotes efficient energy dissipation without the need for excessive reservoir space. In contrast, longer ISBs are more likely to generate periodic submerged jumps, which are less stable and harder to control. Moreover, the results reveal that increasing the normalized ISB length (L/B) and end sill height enhances the velocity reduction and the submergence depth, optimizing the overall energy dissipation performance.

These findings underscore the significant role that ISB geometry plays in determining hydraulic performance and energy dissipation, providing valuable insights for designing efficient energy dissipation structures in hydraulic engineering. These findings are important because they underscore how geometric configurations play a critical role in achieving the desired hydraulic performance. By manipulating these parameters, engineers can tailor ISB designs for specific energy dissipation goals and spatial constraints.

4.3. Role of the Drop Number in ISB Performance

An essential finding of this study is the critical role of the drop number (s/h_1) in the ISB performance. Increasing the drop number for configurations with shorter end sill heights ($h_e/h_c = 0.9$) results in improved velocity reduction (Figs. 7 and 8, and Table 5). The highest performance is achieved at $s/h_1 = 2$, which optimally balances flow dynamics, reduces turbulence, and maximizes energy dissipation. However, for configurations with taller end-sills ($s/h_1 = 1.8$ and 2.7), increasing the drop number beyond $s/h_1 = 2$ provides minimal performance improvement, particularly when submerging the hydraulic jump. This observation is important because it highlights the limits of the influence of the number of drops once the jump becomes submerged, emphasizing the need to carefully consider both the drop number and end sill height in system design. This suggests that while the drop number is critical, its influence is limited when the jump becomes submerged, underscoring the importance of selecting an optimal drop number that avoids overcomplicating the design. This result also addressed the study’s weaknesses by Ohtsu et al. [15].

4.4. Influence of the end sill height on the ISB efficiency

The normalized end sill height (h_e/h_c) is another key factor influencing the ISB efficiency, particularly concerning energy dissipation and velocity reduction (Figs. 9 and 10, and Table 6). Configurations without an end sill (e.g., MND or MNS) performed poorly, achieving only a modest 25 % velocity reduction. However, as the end sill height increases, the performance improves significantly. When $h_e/h_c > 2$, the velocity reduction increases to approximately 60–70 %, indicating a marked improvement in hydraulic efficiency. However, this improvement plateaus beyond an end sill height of $h_e/h_c = 2.7$ to 3.0, where no further significant gains are observed. This is significant because it suggests an optimal range for the end sill height, which maximizes hydraulic efficiency without introducing excessive backflow or complicating construction. This suggests an optimal range for the end sill height, typically between $h_e/h_c = 2.0$ and 2.7, where it maximizes energy dissipation without introducing excessive backflow or complicating construction.

4.5. Velocity reduction and streamline behavior

The velocity profiles along the ISB centerline provide further insight into the influence of the drop number and end sill height on the flow behavior. As shown in Fig. 8, optimized configurations, including those with the appropriate drop number and end sill height, lead to significant reductions in the streamwise velocity, indicating better control of the hydraulic jump. For taller-end sills, the reduction in velocity is even more pronounced, demonstrating that higher-end sill heights offer better control over the hydraulic jump and more efficient energy dissipation. These findings are important because they provide quantitative evidence of how the end sill height and drop number can be optimized to maximize energy dissipation and improve hydraulic jump stability. Fig. 9b and c further confirm that increasing the end sill height above $h_e/h_c = 2.0$ stabilizes the water column above the end sill without causing significant changes in the submergence depth. This stabilization ensures more consistent flow behavior and efficient energy dissipation.

4.6. Optimization of the drop number and end sill height for hydraulic efficiency

Combining an optimum drop number ($s/h_1 = 2$) and a well-chosen end sill height ($h_e/h_c = 2.0$ to 2.7) is essential for balancing energy dissipation and flow stability. These configurations offer the best overall performance, particularly for shorter and moderate end sill heights. As the study shows, while taller end sill heights enhance velocity reduction, there is a point of diminishing returns, particularly above $h_e/h_c = 2.7$, where further increases in the end sill height yield minimal additional benefits. This finding is significant because it suggests an optimal range for the end sill height that maximizes hydraulic performance while avoiding unnecessary complexity and cost in construction. The study also suggests that carefully selecting the drop number and end sill height can reduce excavation and construction costs while ensuring the system operates efficiently. This makes the system hydraulically effective and cost-effective, contributing to the overall feasibility of designing energy dissipation structures in hydraulic engineering applications.

4.7. Challenges in implementing the proposed ISB designs in real-world scenarios

The implementation of the proposed ISB designs in real-world scenarios presents several challenges that must be addressed for successful deployment [53]. First, site-specific conditions, such as variable geological formations, fluctuating inflows, and sediment dynamics, significantly impact the feasibility and efficiency of ISB design. These conditions can lead to variations in the system's hydraulic performance, making it difficult to guarantee consistent energy dissipation and flow

stability over time. Moreover, integrating ISBs into existing infrastructure may be constrained by spatial limitations, particularly for dams with pre-established designs, which require careful retrofitting and adaptation to avoid disruptions. Another challenge lies in the substantial initial construction costs and the ongoing maintenance needs associated with ISBs. Installing features such as cross-walls, modification of the basin length, and sediment management systems involves considerable investment and operational costs. The need for regular monitoring and sediment removal further adds to long-term maintenance burdens. Environmental and ecological considerations, such as preserving fish passage and mitigating impacts on local ecosystems, also present significant hurdles. While ISBs can enhance flow control and stability, their design must account for broader ecological impacts, ensuring they do not disrupt aquatic habitats or water quality downstream.

Additionally, regulatory and policy barriers can delay the implementation of ISB designs. The approval process often involves extensive environmental assessments and consultations with various stakeholders, which may result in changes to the original design or delay project timelines. Public perceptions and local community concerns about potential changes in water flow or other environmental factors may also hinder the widespread acceptance of ISB systems. In conclusion, while ISB designs offer promising benefits for reducing flow energy and mitigating downstream erosion, their successful implementation in real-world scenarios requires complex challenges to be addressed. These include adapting to site-specific conditions, managing costs and maintenance, minimizing ecological impacts, and navigating regulatory and community concerns.

4.8. Limitations and future research directions

Even though the optimum design of ISBs is based on clear water conditions, the ISB performance should also be examined in the presence of sediment. In this context, the scouring pattern within an ISB is important. A study of the scouring pattern within an ISB would provide better insight into the self-cleaning ability (self-flushing) of an ISB and the symmetry and stability of the flow within it. Moreover, it reveals those areas at the apron of the ISB where additional protection, such as steel plates, needs to be considered. This protection is needed to avoid damage to the ISB structure due to dynamic hydraulic forces and sediment transportation.

5. Conclusion

This experimental study provides a comprehensive discussion of the flow behavior within an ISB. The possible hydraulic jumps within ISBs were classified into five types based on their surface patterns and water surface profiles. A steady submerged hydraulic jump is the most effective jump type regarding velocity reduction, stability, and symmetry. By considering the effects of various combinations of ISB geometries on the flow field characteristics within the ISB as well as the ISB performance, the following conclusions can be drawn:

- 1) Increasing the height of the end sill can minimize the velocity figure within the ISB more than if a shorter end sill was used. The length scale for the studied Froude numbers is between 2.5 and 5.5 H, so the normalized end sill height is between 1.8 and 2. Among the values of N, N equal to 7 is the most suitable for energy dissipation, stability, and flow symmetry. Additionally, the flow pattern of the ISB depends more on the end sill height than on the changes in the Froude number and other hydraulic conditions of the upstream river.
- 2) Although a tall end sill at the downstream end of the ISB could stabilize the hydraulic jump, a taller end sill negatively accelerates the downstream velocity because of the free fall flow over the end sill. Therefore, this research recommends selecting the taller end sill while considering the optimum free space at the lateral side of the

- end sill. These free spaces could decrease the free fall rate over the end sill and create a downstream water flow base to prevent erosion.
- 3) Considering two free spaces at the lateral sides of the end sill (slit type) shows almost equal functions for velocity reduction compared with an end sill without free spaces and positively provides additional effects for fish and sediment passing.
 - 4) A medium ISB depth can improve the velocity reduction, whereas further increasing the depth does not improve the velocity reduction and is not cost-effective. In the range of Froude numbers studied in this research, $Fr = 2.5\text{--}5.5$, the drop number equal to 2, and $s/h_1 = 2$ resulted in the greatest energy dissipation.
 - 5) The optimum geometry of the ISB was as follows: $2 < h_e/h_c < 3$, $s/h_1 = 2$, and $L/B = 2$ for a Froude number range between 2.5 and 5.5.
 - 6) Taller end sills and free spaces can improve the self-cleaning process within the ISB. Furthermore, free spaces can provide a symmetric flow pattern within the ISB by artificially reducing the expansion ratio.
 - 7) Increasing the end sill height above an optimum value did not enhance the performance of the ISB. The scour pattern in the case of free spaces was symmetric; however, in the case of the full end sill, the scour pattern was asymmetric.

Free spaces generally reduces the subsequent depth but increases the symmetry and flow stability. In addition to increasing the symmetry and stability of flow within the ISB by considering the free spaces, other important advantages are also provided, such as higher flushing efficiency, fish passage, and improvement of flow conditions downstream of the ISB. The results of this study provide a foundation for practical recommendations and design guidelines for ISBs downstream of flood mitigation dams.

Notation

ASJ	= Asymmetric spatial jump (-)
b_1	= Bottom outlet opening width (m)
b_e	= Effective width of the end sill (m)
B	= In-ground Stilling Basin (ISB) width (m)
BJ	= B-Jump (-)
CHJ	= Classical hydraulic jump (-)
Fr_1	= Upstream Froude number (Fr) at the face of the bottom outlet (-)
Fr_4	= Froude number (Fr) at section IV (-)
FHJ	= Forced hydraulic jump (-)
FMD	= flood mitigation dam (-)
F-SJ	= forced submerged jump (-)
g	= Gravitational acceleration (m/s^2)
h_1	= Bottom outlet opening height (m)
h_2	= Sequent depth (m)
h_3	= Submergence depth (m)
h_e	= Height of the cross wall (m)
h_c	= Critical depth (m)
H_w	= Water head (m)
HP	= Hydraulic Performance (-)
ISB	= In-Ground Stilling Basin (-)
k	= b_1/B = Expansion ratio (-)
L	= In-Ground Stilling Basin (ISB) length (m)
Max B-jump	= Maximum B-jump (-)
NHP	= Normalized Hydraulic Performance (-)
PSJ	= Periodic submerged jump (-)
R	= Reynolds number (-)
Q	= Flow discharge (m^3/s)
S	= Drop depth (also called step height) (m)
S	= s/h_1 = Drop number (-)
SSJ	= Tall End Sill Jump (-)
T-jump	= Transitional Jump (-)
U_0	= Initial velocity at the face of the bottom outlet (m/s)
U_2	= Maximum mean velocity at section II (m/s)
UJ	= Undulated Jump (-)
U_x	= Local streamwise velocity (m/s)
W	= Weber number (-)
W-jump	= Wave Jump (-)

(continued on next column)

(continued)

ASJ	= Asymmetric spatial jump (-)
(X)SM	= Configuration with shallow drop height ($s/h_1 = 1$) and medium end sill height ($h_e/h_c = 0.9$).
(X)SD	= Configuration with deep drop height ($s/h_1 = 1.5$) and medium end sill height ($h_e/h_c = 0.9$).
(X)MM	= Configuration with shallow drop height ($s/h_1 = 1$) and moderate end sill height ($h_e/h_c = 1.8$).
(X)MD	= Configuration with deep drop height ($s/h_1 = 1.5$) and moderate end sill height ($h_e/h_c = 1.8$).
h_e/h_c XTM	= Configuration with shallow drop height ($s/h_1 = 1$) and tall end sill height ($h_e/h_c = 2.7$).
(X)TD	= Configuration with deep drop height ($s/h_1 = 1.5$) and tall end sill height ($h_e/h_c = 2.7$).
y_1	= Depth of the flow at the outflow section (subsequent flow depth, m)
y_2	= Depth of the flow at the inflow section (initial flow depth, m)
Y_2	= h_2/h_1 = Normalized sequential depth (-)
Y_3	= h_3/h_1 = Normalized submergence depth (-)
ρ	= Water density (kg/m^3)
σ	= Surface tension (N/m)
μ	= Dynamic viscosity ($kg/m.s$)

CRedit authorship contribution statement

Ebi Meshkati: Writing – review & editing, Visualization, Validation, Software, Resources, Methodology, Investigation, Formal analysis, Data curation, Conceptualization. **Sameh A. Kantoush:** Writing – review & editing, Writing – original draft, Supervision, Resources, Project administration, Funding acquisition. **Tetsuya Sumi:** Supervision, Resources, Project administration, Investigation, Funding acquisition. **Binh Quang Nguyen:** Writing – review & editing, Writing – original draft, Visualization, Formal analysis, Data curation, Conceptualization. **Hossein Sohrabzadeh Anzani:** Writing – review & editing, Writing – original draft, Validation, Data curation, Conceptualization.

Declaration of competing interest

The authors declare no competing interests.

Acknowledgments

This work was funded by the Japan-ASEAN Science, Technology, and Innovation Platform (JASTIP), the Research Unit for Realization of Sustainable Society (RURSS) at Kyoto University, the JSPS Core-to-Core Program (grant number: JPJSCCB20220004), and JST NEXUS, Japan (Grant Number: JPMJNX24A2). Binh Quang Nguyen is supported by the JSPS Postdoctoral Fellowships Program (Fellowship ID: P24064).

Data availability

Data will be made available on request.

References

- [1] S.A. Kantoush, T. Sumi, Influence of stilling basin geometry on flow pattern and sediment transport at flood mitigation dams, in: 9th FISC, The Federal Interagency Sedimentation Conferences, Las Vegas, Nevada, 2010, pp. 115–133. http://ecohyd.dpri.kyoto-u.ac.jp/content/files/sumi-paper/2010/c8C_Kantoush_02_17_10_paper.pdf.
- [2] G.M. Kondolf, Y. Gao, G.W. Annandale, G.L. Morris, E. Jiang, J. Zhang, Y. Cao, P. Carling, K. Fu, Q. Guo, R. Hotchkiss, C. Peteuil, T. Sumi, H.W. Wang, Z. Wang, Z. Wei, B. Wu, C. Wu, C.T. Yang, Sustainable sediment management in reservoirs and regulated rivers: experiences from five continents, *Earth. Futur.* 2 (5) (2014) 256–280.
- [3] M.E. Meshkati Shahmirzadi, T. Sumi, Hydraulic design of in-ground stilling basin under submerged jump conditions for flood mitigation dams, *J. Jpn. Soc. Civi. Eng., Ser. B1 (Hydraul. Eng.)* 69 (4) (2013), https://doi.org/10.2208/jscejhe.69.1_79.1_79-1_84.
- [4] T. Sumi, S.A. Kantoush, A. Shirai, Worldwide Flood Mitigation Dams: Operating and Designing Issues, 2011 na, <http://ecohyd.dpri.kyoto-u.ac.jp/content/files/sumi-paper/2011/c22367.pdf>.

- [5] F. Lempérière, The role of dams in the XXI century: achieving a sustainable development target, *Int. J. Hydropow. Dam.* 13 (3) (2006) 99–108, <https://doi.org/10.1201/b16818-165>.
- [6] H. Sohrabzadeh-Anzani, M. Ghodsian, Energy dissipation of rectangular and trapezoidal piano key weir, *Irrigat. Drainage Struct. Eng. Res.* 24 (90) (2023) 17–32, <https://doi.org/10.22092/idser.2023.362286.1545>, a.
- [7] H. Sohrabzadeh Anzani, M. Ghodsia, Energy dissipation of triangular piano key weir, *J. Hydraul.* 18 (3) (2023) 35–44, <https://doi.org/10.30482/jhyd.2023.365692.1622>, b.
- [8] H. Sohrabzadeh Anzani, M. Ghodsian, Comparison of discharge capacity of piano key weir with ogee and sharp crest weirs, *Modar. Civi. Eng. J.* 23 (5) (2023) 129–138, <https://doi.org/10.22034/23.5.9>, c.
- [9] M. Aydogdu, E. Gul, O.F. Dursun, Experimentally verified numerical investigation of the sill hydraulics for abruptly expanding stilling basin, *Arab. J. Sci. Eng.* 48 (4) (2023) 4563–4581, <https://doi.org/10.1007/s13369-022-07089-6>.
- [10] S. Kantoush, T. Sumi, M. Meshkati, Eco-friendly hydraulic design of in-stream flood mitigation dams, *Environ. Sci. Eng.* 54 (B) (2011) 735–745, <http://hdl.handle.net/2433/151019>.
- [11] A. Rabbiei, J. Mohammadzadeh-Habili, A.A. Chadee, S.M. Zomorodian, M. Jameel, H.M. Azamathulla, Performance of a right-triangle stilling basin: a laboratory investigation, *Water Supply* 23 (9) (2023) 3912–3924, <https://doi.org/10.2166/ws.2023.209>.
- [12] G.B. Ferreri, C. Nasello, Hydraulic jumps at drop and abrupt enlargement in rectangular channel, *J. Hydraul. Res.* 40 (4) (2002) 491–504, <https://doi.org/10.1080/002216802209499891>.
- [13] M. Mossa, A. Petrillo, H. Chanson, Tail water level effects on flow conditions at an abrupt drop, *J. Hydraul. Res.* 41 (1) (2003) 39–51, <https://doi.org/10.1080/00221680309499927>.
- [14] I. Ohtsu, Y. Yasuda, Transition from supercritical to subcritical flow at an abrupt drop, *J. Hydraul. Res.* 29 (3) (1991) 309–328, <https://doi.org/10.1080/00221689109498436>.
- [15] I. Ohtsu, Y. Yasuda, M. Ishikawa, Submerged hydraulic jumps below abrupt expansions, *J. Hydraul. Eng.* 125 (5) (1999) 492–499, [https://doi.org/10.1061/\(ASCE\)0733-9429\(1999\)125:5\(492\)](https://doi.org/10.1061/(ASCE)0733-9429(1999)125:5(492)).
- [16] P. Parsamehr, D. Farsadzadeh, A. Hosseinzadeh Dalir, A. Abbaspour, M.J. Nasr Esfahani, Characteristics of hydraulic jump on rough bed with adverse slope, *ISH J. Hydraul. Eng.* 23 (3) (2017) 301–307, <https://doi.org/10.1080/09715010.2017.13143>.
- [17] S. Pagliara, Wave type flow at abrupt drop: flow geometry and energy loss. *Entropy and Energy Dissipation in Water Resources*, Springer, Netherlands, 1992, pp. 469–479. https://hal.science/hal-04445744v1/file/LMFL_JFM_2023_LIU_Sh_uo.pdf.
- [18] S.K. Kunsztow, Die Fließbewegung bei plotzlicher Verbreiterung des Strombettes, *Gidrotechniceskoe Stroitelstvo* 27 (6) (1958) 34–37.
- [19] W.H. Hager, Hydraulic jump in non-prismatic rectangular channels, *J. Hydraul. Res.* 23 (1) (1985) 21–35.
- [20] R. Bremen, W.H. Hager, Expanding stilling basin, *Proc., ICE Water Marit. Eng.* 106 (3) (1994) 215–228. https://www.researchgate.net/publication/37455753_Expanding_stilling_basin.
- [21] M.N. Hasani, K. Nekoufar, M. Biklarian, M. Jamshidi, Q.B. Pham, D.T. Anh, Investigating the pressure fluctuations of hydraulic jump in an abrupt expanding stilling basin with roughened bed, *Water* 15 (1) (2023) 80, <https://doi.org/10.3390/w15010080>.
- [22] K. Herbrand, J. Knauss, *Computation and Design of Stilling Basins With Abruptly Or Gradually Enlarged Boundaries*, Commission Internationale des Grands Barrages, 1973.
- [23] T.E. Unny, The spatial hydraulic jump, in: *Proc. 10th Congress of IAHR*, London, 1963, pp. 32–42, <https://doi.org/10.1080/00221687309499774>.
- [24] H.K. Zare, J.C. Doering, Forced hydraulic jumps below abrupt expansions, *J. Hydraul. Eng.* 137 (8) (2011) 825–835, [https://doi.org/10.1061/\(ASCE\)HY.1943-7900.0000369](https://doi.org/10.1061/(ASCE)HY.1943-7900.0000369).
- [25] N. Afzal, A. Seena, A. Bushra, Analysis of turbulent hydraulic jump over a transitional rough bed of a rectangular channel: universal relations, *J. Eng. Mech. ASCE* 137 (2011) 835–845, [https://doi.org/10.1061/\(ASCE\)EM.1943-7889.0000294](https://doi.org/10.1061/(ASCE)EM.1943-7889.0000294).
- [26] A. Abbaspour, A.H. Dalir, D. Farsadzadeh, A.A. Sadraddini, Effect of sinusoidal corrugated bed on hydraulic jump characteristics, *J. Hydroenviron. Res.* 3 (2) (2009) 109–117, <https://doi.org/10.1016/j.jher.2009.05.003>.
- [27] H.M.A. Ahmed, M. El Gendy, A.M.H. Miridan, A.A.M. Ali, F.S.F.A. Haleem, Effect of corrugated beds on characteristics of submerged hydraulic jump, *Ain Shams Eng. J.* 5 (4) (2014) 1033–1042, <https://doi.org/10.1016/j.asej.2014.06.006>.
- [28] F.G. Carollo, V. Ferro, V. Pampalone, Hydraulic jumps on rough beds, *J. Hydraul. Eng.* 133 (9) (2007) 989–999, [https://doi.org/10.1061/\(ASCE\)0733-9429\(2007\)133:9\(989\)](https://doi.org/10.1061/(ASCE)0733-9429(2007)133:9(989)).
- [29] S.A. Ead, N. Rajaratnam, Hydraulic jumps on corrugated beds, *J. Hydraul. Eng.* 128 (7) (2002) 656–663, [https://doi.org/10.1061/\(ASCE\)0733-9429\(2002\)128:7\(656\)](https://doi.org/10.1061/(ASCE)0733-9429(2002)128:7(656)).
- [30] W.C. Hughes, J.E. Flack, Hydraulic jump properties over a rough bed, *J. Hydraul. Eng.* 110 (12) (1984) 1755–1771, [https://doi.org/10.1061/\(ASCE\)0733-9429\(1984\)110:12\(1755\)](https://doi.org/10.1061/(ASCE)0733-9429(1984)110:12(1755)).
- [31] S. Pagliara, I. Lotti, M. Palermo, Hydraulic jump on rough bed of stream rehabilitation structures, *J. Hydroenviron. Res.* 2 (1) (2008) 29–38, <https://doi.org/10.1016/j.jher.2008.06.001>.
- [32] N. Rajaratnam, Hydraulic jumps on rough beds, *Trans. Eng. Inst. Can.* 11 (A-2) (1968) 1–8, [https://doi.org/10.1061/\(ASCE\)0733-9429\(2007\)133:9\(989\)](https://doi.org/10.1061/(ASCE)0733-9429(2007)133:9(989)).
- [33] S. Koley, Role of fluid dynamics in infectious disease transmission: insights from COVID-19 and other pathogens, *Trend. Sci.* 21 (8) (2024) 8287, <https://doi.org/10.48044/tis.2024.8287>.
- [34] H. Chanson, R. Carvalho, *Hydraulic jumps and stilling basins. Energy Dissipation in Hydraulic Structures*, CRC Press, Leiden, The Netherlands, 2015, pp. 65–104.
- [35] J.N. Bradley, A.J. Peterka, Hydraulic design of stilling basins: Hydraulic jumps on a horizontal apron (Basin D), *J. Hydraul. Divis.* 83 (5) (1957) 1–1401, <https://doi.org/10.1061/JYCEAJ.0000126>.
- [36] N. Rajaratnam, K.I. Hurlig, Screen-type energy dissipator for hydraulic structures, *J. Hydraul. Eng.* 126 (4) (2000) 310–312.
- [37] M. Debabeche, M. Lakehal, N. Mansri, B. Achour, Theoretical study of the forced hydraulic jump by positive step in a triangular channel, *Int. J. Fluid Mech. Res.* 35 (4) (2008), <https://doi.org/10.1615/InterJFluidMechRes.v35.i4.20>.
- [38] J. Maatoog, The effects of baffle blocks locations and blockage ratio on the sequent depth and velocity distribution of forced hydraulic jump, in: *7th IAHR International Symposium on Hydraulic Structures*, Aachen, Germany, 2018.
- [39] G. Mahtabi, B. Chaplot, H.M. Azamathulla, M. Pal, Classification of hydraulic jump in rough beds, *Water* 12 (8) (2020) 2249, <https://doi.org/10.3390/w12082249>.
- [40] U. Türker, M. Valyrakis, Hydraulic jump on rough beds: conceptual modeling and experimental validation, *Water Supply* 21 (4) (2021) 1423–1437, <https://doi.org/10.2166/ws.2020.292>.
- [41] R. Bai, R. Ning, S. Liu, H. Wang, Hydraulic jump on a partially vegetated bed, *Water Resour. Res.* 58 (7) (2022), <https://doi.org/10.1029/2022WR032013>.
- [42] D. De Padova, M. Mossa, Hydraulic jump: a brief history and research challenges, *Water* 13 (13) (2021) 1733, <https://doi.org/10.3390/w13131733>.
- [43] C. Abdi Chooplou, E. Bodaghi, M. Ghodsian, M. Vaghefi, Temporal evolution of scouring downstream of a trapezoidal piano key weir, *Int. J. River Basin Manag.* 22 (3) (2024) 351–364.
- [44] H. Sohrabzadeh Anzani, M. Ghodsian, Experimental study of flow over piano key weirs with different plan shapes, *ISH J. Hydraul. Eng.* 30 (2) (2024) 185–195, <https://doi.org/10.1080/09715010.2024.2302808>.
- [45] H. Sohrabzadeh Anzani, S.A. Kantoush, A. Mahdian Khalili, M. Hamidi, Energy dissipation assessment in flow downstream of rectangular sharp-crested weirs, *Water* 16 (23) (2024) 3371, <https://doi.org/10.3390/w16233371>, a.
- [46] H. Sohrabzadeh Anzani, S.A. Kantoush, A. Mahdian Khalili, M. Hamidi, Experimental investigation of slit weir discharge, *ISH J. Hydraul. Eng.* 30 (5) (2024) 645–654, <https://doi.org/10.1080/09715010.2024.2401845>, b.
- [47] M. Ghodsian, H. Sohrabzadeh Anzani, Experimental study on flow over rectangular Piano key weirs with sloped side crests, *Modar. Civi. Eng. J.* 23 (2) (2023) 167–175, <https://doi.org/10.22034/23.2.11>.
- [48] A.M. Khalili, M. Hamidi, P.A. Dadamahalleh, Experimental study of the effect of rectangular debris blockage on the scour hole development around a cylindrical bridge pier, *Water Pract. Technol.* 19 (5) (2024) 1878–1892.
- [49] Y. Sangsefidi, H. Tavakol-Davani, M. Ghodsian, M. Mehraein, R. Zarei, Hydrodynamics and free-flow characteristics of piano key weirs with different plan shapes, *Water* 13 (15) (2021) 2108, <https://doi.org/10.3390/w13152108>.
- [50] S. Kiani, M. Fathimoghadam, R. Behroozirad, L. Davoodi, Control of hydraulic jump in the stilling basins with perforated sill, *Irrigat. Water Eng.* 7 (4) (2017) 26–36.
- [51] V. Heller, Scale effects in physical hydraulic engineering models, *J. Hydraul. Res.* 49 (3) (2011) 293–306, <https://doi.org/10.1080/00221686.2012.654671>.
- [52] J.F. Macián-Pérez, F.J. Vallés-Morán, R. García-Bartual, Assessment of the performance of a modified USBR Type II stilling basin by a validated CFD model, *J. Irrigat. Drain. Eng.* 147 (11) (2021) 04021052, [https://doi.org/10.1061/\(asce\)ir.1943-4774.0001623](https://doi.org/10.1061/(asce)ir.1943-4774.0001623).
- [53] H. Wang, R. Tang, Z. Bai, S. Liu, W. Sang, R. Bai, Prototype air–water flow measurements in D-type hydraulic jumps, *J. Hydraul. Res.* 61 (1) (2023) 145–161, <https://doi.org/10.1080/00221686.2022.2132310>.